Manuscript version April 26th, 2020

Parkinson Disease-Linked Parkin Mediates Redox Reactions That Lower Oxidative Stress In Mammalian Brain

Daniel N. El Kodsi[1,2]*, Jacqueline M. Tokarew[1,2]*, Rajib Sengupta[3,3^], Nathalie A. Lengacher[1], Andy C. Ng[1], Heather Boston[1], Qiubo Jiang[1], Carina Palmberg[3], Chantal Pileggi[4], Bojan Shutinoski[1], Juan Li[1], Angela P. Nguyen[1], Travis K. Fehr[1,2], Doo Soon Im[2,2^], Steve Callaghan[2], David S. Park[2,2^], Matthew J. LaVoie[5], Jennifer A. Chan[6,6^], Masashi Takanashi[7], Nobutaka Hattori[7], Rajiv R. Ratan[8], Luigi Zecca[9], Lawrence Puente[10], Gary S. Shaw[11], Mary-Ellen Harper[4], Arne Holmgren[3%], Julianna J. Tomlinson[1,12]#, and Michael G. Schlossmacher[1,2,12,13]#

[1]Program in Neuroscience, Ottawa Hospital Research Institute, Ottawa, ON, Canada

[2]Department of Cellular and Molecular Medicine ([2^]Present address: Hotchkiss Brain Institute, University of Calgary, Calgary, AB, Canada), and

[4]Department of Biochemistry, Microbiology and Immunology Faculty of Medicine, and Ottawa Institute of Systems Biology, University of Ottawa, Ottawa, ON, Canada

[3]Department of Biochemistry, Karolinska Institute, Stockholm, Sweden; [3^]Present Address: Amity Institute of Biotechnology, Amity University, Kolkata, West Bengal, India

[5]Ann Romney Center for Neurologic Diseases, and [6]Department of Pathology, Brigham and Women's Hospital, Boston, MA, USA; [6^]Present Address: Department of Pathology and Laboratory Medicine, University of Calgary, Calgary, AB, Canada

[7]Department of Neurology, Juntendo University School of Medicine, Tokyo, Japan

[8]Department of Neurology, Burke Rehabilitation Institute, Weill-Cornell College of Medicine, New York, NY, USA

[9]Institute of Medical Technologies, Italian National Research Council, Milan, Italy

[10]Proteomics Core Facility, Ottawa Hospital Research Institute, Ottawa, ON, Canada

[11]Department of Biochemistry, University of Western Ontario, London, ON, Canada

[12]University of Ottawa Brain and Mind Research Institute, Ottawa, ON, Canada

[13]Division of Neurology, Department of Medicine, The Ottawa Hospital, Ottawa, ON, Canada

*These authors contributed equally to this work; [%]deceased

#Lead contacts: jtomlins@uottawa.ca; mschlossmacher@ohri.ca

SUMMARY

We recently hypothesized that parkin plays a role in redox homeostasis and provided evidence that it directly reduces hydrogen peroxide (H_2O_2) *in vitro*. Here, we examined this anti-oxidant activity *in vivo*. Informed by findings in human brain, we demonstrate that elevated oxidative stress promotes parkin insolubility in mice. In normal mouse brain parkin was partially oxidized, *e.g.,* at cysteines 195 and 252, which was augmented by oxidative stress. Although under basal conditions H_2O_2 levels were unchanged in adult *prkn*$^{-/-}$ brain, a parkin-dependent reduction of cytosolic H_2O_2 was observed when mitochondria were impaired, either due to neurotoxicant exposure (MPTP) or *Sod2* haploinsufficiency. In accordance, markers of oxidative stress, *e.g.,* protein carbonylation and nitrotyrosination, were elevated in the cytosol but not in mitochondria from *prkn*$^{-/-}$ mice. This rise in oxidative stress was associated with altered glutathione homeostasis. In parkin's absence reduced glutathione concentrations were increased in cells, murine brain and human cortex. This compensation was not due to new glutathione synthesis but attributed to elevated oxidized glutathione (GSSG)-reductase activity. Moreover, we discovered that parkin also recycled GSSG to its reduced form. With this reaction, parkin became S-glutathionylated, *e.g.,* at cysteines 59 and human-specific 95. This oxidative modification was reversed by glutaredoxin. Our results demonstrate that cytosolic parkin mediates anti-oxidant reactions including H_2O_2 reduction and glutathione regeneration. These reducing activities lead to a range of oxidative modifications in parkin itself. In parkin-deficient brain oxidative stress rises despite changes to maintain redox balance.

239 words

INTRODUCTION

Parkinson disease (PD) is a progressive, heterogeneous disorder of the human brain that remains incurable. Young-onset, autosomal-recessive PD (ARPD) due to deficiency in parkin (encoded by *PRKN*) is restricted to the degeneration of dopaminergic neurons in the *S. nigra* and *L. coeruleus*[1,2]. In the ageing human brain, these neurons are susceptible to degeneration owing to unique features. These include: extensive arborization; a high number of mitochondria within each axon; the presence of metals like iron and copper in redox-reactive form[3]; ongoing generation of toxic dopamine metabolites in the cytosol; a greater need to buffer Ca^{2+} ions; and collectively, a greater degree of oxidative stress[4-6].

Parkin is a principally cytosolic, RING-carrying protein with ubiquitin ligase activity and is involved in the regulation of mitophagy and immune-related functions[7,8 9]. The role for each of these functions in relation to the development of ARPD in adults, however, remains unknown. We have recently described that parkin itself is highly oxidized in human brain in part due to its many cysteines, and discovered that it can act as a redox molecule to decrease dopamine metabolism-associated stress[10,11].

Oxidative stress and mitochondrial damage have been implicated in the pathogenesis of several brain diseases including PD[12]. Mitochondrial dysfunction, as induced by neurotoxicants, *e.g.*, 1-methyl-4-phenyl-1,2,3,6-tetrahydropyridine (MPTP) and rotenone, augments oxidative stress[13]. The integrity of the cellular thiol pool, a network formed by glutathione and the cysteine proteome, is essential in maintaining redox homeostasis and thus to the survival of long-lived, post-mitotic neurons. Reduced glutathione (GSH) plays a critical role as an anti-oxidant, as co-factor of enzymes, and as a reservoir of cellular thiols. Accordingly, a chronic decline in GSH has been implicated in many human disorders including neurodegenerative diseases[14].

Genomic deficiency in parkin in mice does not lead to loss of dopamine neurons, and *prkn*$^{-/-}$ animals do not develop parkinsonism. However, unbiased studies have revealed significant proteomic changes in these animals[15,16]. There, we noted that the majority of dysregulated proteins in the brain, which showed altered isoelectric points on 2D-gels,

had been previously identified as enzymes (55/92; 59.8%). Many of the proteins were also known as redox-sensitive proteins (72/92; 78.2%), *e.g.*, peroxiredoxins, glyoxalase and aconitase-2[15,16]. This finding suggested to us that posttranslational modifications, rather than changes in protein abundance, could have explained their dysregulation.

When taken together with previous reports of parkin's sensitivity to pro-oxidants[10,17], we hypothesized that: one, thiol-rich parkin is altered in response to cellular redox changes; two, parkin itself plays a role in lowering oxidative stress *in vivo*, thus influencing redox-state and redox-sensitive enzymes; and three, the loss of parkin's anti-oxidant effects contributes to mitochondrial changes. We therefore characterized parkin's redox activity *in vitro*, explored the downstream oxidative changes in cells and mouse models with low or absent parkin expression, and investigated parkin's effect on the thiol network. This work was informed by parallel efforts, which focused on parkin's processing in human midbrain and its role in dopamine metabolism[11].

RESULTS

Mitochondrial and cytosolic stress conditions lead to oxidation of cellular parkin

Using cell-based paradigms, we first analyzed parkin's response to cytosolic and mitochondrial stressors. Chinese hamster ovary cells that stably express wild-type (WT) human *PRKN* cDNA (CHO-parkin) and control cells, which in our hands showed little detectable, endogenous parkin by routine Western blotting, were exposed to different levels of hydrogen peroxide (H_2O_2, 0.2 or 2mM) or carbonyl-cyanide-m-chlorophenyl-hydrazine (CCCP, 10μM). Under these stress conditions, which did not cause cell death, we observed the time-dependent loss of parkin's monomer (~52.5 kDa) and an increase in high molecular weight (HMW) species (**Fig. 1a**)[17]. These biochemical changes were seen under non-reducing gel electrophoresis conditions and thus interpreted as involving parkin thiol-based oxidation. Intriguingly, this oxidation was specific to parkin as endogenous, redox-sensitive and ARPD-linked Dj-1[18] did not undergo similar changes (**Fig. 1a**).

In oxidative stress-exposed, human embryonic kidney (HEK293) cells, which transiently over-expressed *PRKN*, we also observed HMW smear formation. Parkin became progressively gel excluded (aggregated) and insoluble following exposure to higher levels of H_2O_2 (**Fig. 1b**). Since these HMW forms of parkin were reversed with dithiothreitol (DTT; **Extended Data Fig. 1a, c**), we postulated that these modifications occurred due to increasing oxidation of parkin's cysteines[17]. We tested this using N-ethylmaleimide (NEM) and iodoacetamide (IAA), which irreversibly alkylate free thiols. There, we found that pre-incubation of cells with NEM or IAA blocked HMW smear formation of parkin and preserved its solubility during H_2O_2 stress (**Fig. 1b; Extended Data Fig. 1b**). Complementing these findings, we mapped several cysteines in recombinant (r-) parkin, which became oxidized when the protein was subjected to rising H_2O_2 levels *in vitro*, thereby promoting its aggregation and insolubility[11].

Intriguingly, exposure to DTT also lowered the solubility of cellular parkin (**Extended Data Fig. 1c**), which suggested that parkin's structure is altered under excessive oxidizing and excessive reducing conditions. These results demonstrated that human parkin acts as a redox-sensitive molecule, which undergoes thiol chemistry-based changes in cells during redox stress.

Excessive ROS exposure in mice promotes parkin insolubility

Under stress-free conditions, parkin resides in the cytosol of cells (**Fig. 1a, b**) and rodent brain[19,20]. In contrast, in human control brain parkin is largely insoluble after the 4th decade of life[11,20]. To better understand the link between parkin's oxidation and insolubility, we sought to validate our findings from cellular work (above) and human brain analyses[11] in mice. We tested this in three ways. First, freshly dissected brains from WT mice were homogenized either in the presence or absence of H_2O_2 to generate high amounts of reactive oxidative species (ROS). Lysates were then fractionated and separated into soluble *vs.* insoluble fractions; in the latter, proteins were extracted using 2-10% SDS. Exposure to H_2O_2 *in situ* led to a significant loss in solubility of mouse parkin and its recovery in the insoluble fraction ($P<0.001$), as monitored by reducing SDS/PAGE. No such shift was observed for murine Dj-1 (**Fig. 1c, d**).

Secondly, we examined parkin's response to oxidative stress *in vivo*. We injected a single dose of the neurotoxicant MPTP into the peritoneum of adult mice at a dose (40mg/kg) that induces oxidative stress without causing neuronal death[21]. After one hour, brains were collected and serially fractionated. The brief exposure to MPTP led to a decline of >50% in soluble parkin when compared to saline-treated controls. As expected, parkin's detection rose in the insoluble fraction ($P<0.05$; **Fig. 1e; Extended Data Fig. 1d, e**).

In a third approach, we tested whether a genetically induced, mitochondrial defect altered parkin solubility. We chose *Sod2*$^{+/-}$ haploinsufficient mice with lower expression of mitochondrial superoxide dismutase-2 (aka MnSOD). Reduced MnSOD2 activity (**Extended Data Fig. 1h, i**) results in systemically elevated oxidative stress[22]. As expected, we detected a parkin solubility shift in adult *Sod2*$^{+/-}$ brain ($P<0.05$; **Fig. 1f**; **Extended Data Fig. 1j, k**). We concluded that toxicologically and genetically induced, oxidative stress led to parkin insolubility in the brain. We postulated that this change corresponded with fewer free thiols, due to increased oxidation, within parkin itself.

Exposure to MPTP increases parkin oxidation in the brain

To determine whether oxidative modifications could be identified in murine parkin, we employed liquid chromatography coupled to mass spectrometry (LC-MS/MS). Brains from animals injected either with MPTP or saline (as above) were homogenized in the presence of IAA to alkylate free cysteines and prevent thiol oxidation during processing. Parkin-enriched isolates were separated by SDS/PAGE (**Extended Data Fig. 1f**). There, monomeric, alkylated parkin was gel-excised, trypsin digested and subjected to LC-MS/MS. We recorded a <20% decline in the relative amounts of unmodified cysteines in parkin peptides from MPTP-treated mice compared to those from saline-injected controls (**Extended Data Table 1**). Furthermore, we found that select cysteines had been oxidized *in vivo* even under normal conditions, *e.g.*, to dehydroalanine, sulfinic acid and sulfonic acid (**Extended Data Table 1**). Intriguingly, residues C195 and C252 were frequently identified as irreversibly oxidized, under both basal and oxidized conditions, suggesting oxidation of parkin occurred physiologically in mouse brain (**Extended Data Table 1;**

Extended Data Fig. 1g). In parallel studies of human parkin, we found that oxidation of orthologous cysteines, *e.g.*, C253, contributed to parkin's progressive insolubility[11].

Parkin reduces hydrogen peroxide to water in a thiol-dependent manner

We recently provided evidence that WT r-parkin reduced H_2O_2 to water *in vitro* by reciprocal oxidation of its thiol groups[11]; ARPD-linked point mutants did so less well. Here, we further explored the biochemical mechanisms underlying this activity. Wild-type r-parkin was nearly 5-fold more effective in lowering H_2O_2 levels than GSH at equimolar concentrations, but it was less potent than the enzyme catalase (**Extended Data Fig. 2a)**. This suggested that parkin shared a thiol-based anti-oxidant mechanism with GSH. We confirmed this by demonstrating that r-parkin's ability to lower H_2O_2 was abrogated when its thiols were either oxidized prior to the reaction or irreversibly blocked by NEM (**Extended Data Fig. 2b, c**). Furthermore, r-parkin did not exhibit peroxidase-type anti-oxidant activity (**Supp. Fig. 2D**).

Two other PD-linked proteins, *e.g.*, α-synuclein and DJ-1 (with 0 and 3 cysteines, respectively; **Extended Data Fig. 2e**), had no detectable H_2O_2-lowering activity (**Fig. 2a**). Bovine serum albumin with the same number of cysteines as human parkin (n, 35) and two RING-carrying E3 ubiquitin ligases, *e.g.*, RNF43 and HOIP (**Extended Data Fig. 2e, f**), also failed to lower H_2O_2 (**Fig. 2a**). The latter results suggested that parkin's structure played an important role in its activity but was not solely due to the presence of its four RING domains, each of which chelates two Zn^{2+} ions (**Extended Data Fig. 1g**)[23]. As expected, competitive chelation of Zn^{2+} ions by rising EDTA concentrations prior to the reaction diminished r-parkin's antioxidant activity *in vitro*. This was partially, but not completely, reversed when excess Zn^{2+} was added back to the reaction mix (**Extended Data Fig. 2g**). Of note, EDTA and NEM alone had no effect on the assay (**Extended Data Fig. 2h**). We concluded from these findings that parkin's H_2O_2-reducing activity was: not enzymatic, required integrity of its tertiary structure, depended on free thiols, and resembled GSH's mechanism of action.

PRKN expression lowers hydrogen peroxide concentrations in the cytosol

We next asked whether parkin's anti-oxidant activity contributed to redox balance in cells and *in vivo*. Under basal conditions, HEK293-parkin cell lysates showed a trend toward lower levels of H_2O_2 when compared to control cells; the difference became significant when we monitored intact cells (**Fig. 2b** and **Extended Data Fig. 2i**, respectively). When HEK293 cultures were exposed to a rise in oxidative stress, *e.g.*, after CCCP treatment or excessive levels of H_2O_2 due to the presence of aminotriazole (AT, a catalase inhibitor; **Extended Data Fig. 2a**), parkin-expressing cell lysates had a significantly lower level of ROS ($P<0.0001$; **Fig. 2b**).

We next tested parkin's effects on H_2O_2 levels in murine brain using a validated AmplexRed assay (**Extended Data Fig. 2j**). We found that basal ROS concentrations did not markedly differ between adult *prkn*$^{-/-}$ and WT mice, neither in the cytosol nor in isolated mitochondria (**Fig. 2c,d; Extended Data Fig. 3b**). A rise in oxidative stress from exposure to MPTP, however, caused a significant increase in endogenous ROS levels in parkin-deficient mice ($P<0.001$; **Fig. 2e**). Under basal conditions H_2O_2 concentrations were also higher in the cytosol of *Sod2*$^{+/-}$ mutant and bigenic animals (*prkn*$^{-/-}$*//Sod2*$^{+/-}$), which we had created to further increase metabolic stress ($P<0.05$; **Fig. 2c, d**; **Extended Data Fig. 1h, i**). Of note, at the same age *Sod2*$^{+/-}$ and bigenic mice did not show detectable cell loss (data not shown). Unexpectedly, ROS levels remained the same in isolated brain mitochondria from *Sod2*$^{+/-}$ mice, which suggested rapid shuttling of rising superoxide levels from their mitochondria into the cytosol[24].

Prkn gene expression lowers oxidative stress in mammalian brain

We next examined the degree of protein carbonylation, a marker of chronically elevated H_2O_2, in the same mouse lines. Carbonyl content was increased in the cytosol of *prkn*-mutant brain, even under basal conditions, but remained normal in isolated mitochondria. There, we also observed a *prkn*-null allele dosage effect (**Fig. 2f**). As expected, carbonyl content was further increased in the bigenic mice when compared to WT, *prkn*$^{-/-}$ and *Sod2*$^{+/-}$ littermates ($P<0.001$ and $P<0.05$ respectively; **Fig. 2g**). A second marker of oxidative stress-induced protein modification, *i.e.*, nitrotyrosination, was also increased in

the cytosol of heart tissues in these *prkn*$^{-/-}$ mice (**Extended Data Fig. 3c, d**), consistent with a previous report by Palacino et al., who had used a different model[15].

We next compared protein carbonyl content in control subjects *vs.* patients with *PRKN*-linked ARPD (each, n=4). These had been matched for age, *post mortem* interval, ethnicity and hospital morgue (**Extended Data Fig. 3a**)[25]. In the absence of any parkin, the level of protein carbonylation showed a trend toward elevation. Cortices from three, non-*PRKN*-linked parkinsonism cases revealed the same degree of carbonyl content as recorded for age-matched controls (**Fig. 2h**). Using a logistic regression model with the carbonyl content measured in all brains (mouse and human) as the dependent variable, we found that oxidative stress correlated with parkin deficiency; the co-efficient was -0.3754 (95% CI, -0.6611–0.0053; P=0.05; **Fig. 2i**). Of note, in these redox studies, we did not observe any sex effect. Together, these results established that WT parkin contributed to H_2O_2 reduction in cells and brain during both basal activities and during rising oxidative stress.

***Prkn* gene expression affects redox-dependent enzymatic activity**

To link this finding back to proteomic changes downstream of parkin deficiency, we explored redox-dependent enzymatic activity changes. In the brains of *prkn*$^{-/-}$ mice, we found significantly increased activity of aconitase-2 (Aco2), a $NADP^+$-linked enzyme, under basal conditions when compared to littermates (P<0.001; **Fig. 2j**). Following exposure of isolated brain mitochondria to H_2O_2, Aco2 activities were decreased in both WT and *prkn*-null brains, as expected; however, the activity remained measurably higher in *prkn*$^{-/-}$ animals (P<0.05; **Fig. 2j**). Importantly, the levels of murine (and human) Aco2 orthologues were not altered in these brains, neither in whole lysates nor in isolated mitochondria, when compared between the two genotypes (**Extended Data Fig. 3b, e, f**). These findings were consistent with the results by Periquet et al., who had shown that Aco2 undergoes an electrophoretic migration shift in parkin's absence[16]. We concluded that increased cytosolic ROS production in parkin-deficient brain could thus explain the structural, proteomic changes detected in *prkn*$^{-/-}$ animals.

Parkin contributes to the thiol network during oxidative stress

Based on parkin's cysteine-dependent redox activity and its protection against chronic oxidative stress, we questioned whether it confers cellular protection by altering the thiol network. To test this, we first compared survival rates of CHO-parkin cells following exposure to H_2O_2 after depletion of GSH with buthionine sulfoximine (BSO). Treatment with either H_2O_2 (1h) or BSO alone (48hs) did not cause cell death (**Extended Data Fig. 2k**). Under combined stress conditions, *PRKN* expression was protective: it resulted in a significantly lower cell death rate ($P<0.05$; **Fig. 3a**), normalized ROS levels ($P<0.001$; **Fig. 3b**), and led to reciprocal parkin oxidation (Fig. 1A). Treatment with excess n-acetylcysteine as an abundant source of free thiols resulted in similar, protective effects as did *PRKN* expression (**Fig. 3a, b**). Based on these results, we conjectured that parkin supplements the cellular thiol network possibly through its own free thiols, which could neutralize ROS.

***PRKN* gene expression alters glutathione redox state in cells and human brain**

If parkin contributes to the thiol pool directly, we would anticipate that it could lead to an altered GSH redox state. We examined this by directly measuring GSH (reduced) and GSSG (oxidized) concentrations by HPLC. There, CHO-control cells had relatively high concentrations of GSH and low amounts of GSSG, with an elevated ratio of GSH:GSSG (**Fig. 3c**). Increased expression of WT parkin significantly reversed these redox indices ($P<0.01$ and $P<0.001$), but no change was found in the total concentration of GSH and GSSG (**Extended Data Fig. 4a**). Consistent with previously reported findings indicating that CHO cells display high stress tolerance[26], exogenously added H_2O_2 did not substantially change the redox indices between CHO-control and CHO-parkin cells with the exception of now equalized GSSG levels (**Fig. 3d**). Parkin-dependent changes in GSH levels and GSH:GSSG ratios were also observed in transiently transfected HEK293 cells (not shown) and in human, dopaminergic SH-SY5Y cells (**Fig. 3e**).

The interplay between *PRKN* expression and GSH redox state was further validated in human brain using cortex specimens from patients with *PRKN*-linked ARPD and healthy controls (as used above). In the absence of detectable parkin, the level of reduced GSH as

well as the ratio of GSH:GSSG were significantly increased (P<0.01 and P<0.05 respectively). No differences were seen for GSSG levels (**Fig. 3f**) or the total concentration of GSH and GSSG (**Extended Data Fig. 4b**). Intriguingly, the redox changes recorded in human brain therefore closely mirrored those in CHO cells exposed to higher ROS levels (**Fig. 3d**). We concluded that a reciprocal relationship existed between *PRKN* expression and GSH levels *in vivo*. When combining the results from these different paradigms and using a logistic regression model with GSH levels as the dependent variable, we found that low expression of parkin was associated with higher GSH levels; the co-efficient was -0.6889 (95% CI, -0.849 to -0.411; P<0.0001; **Fig. 3g**).

***Prkn* deletion alters glutathione metabolism in mice with a mitochondrial defect**

Two groups previously reported elevated GSH levels in *prkn* $^{-/-}$ mice and their glia[27,28]. When examining the same colony generated by Itier et al. using our HPLC method, parkin-deficient brains showed similar but non-significant trends for thiol changes, *i.e.* higher concentrations of reduced GSH, lower levels of GSSG, and a higher GSH:GSSG ratio (**Fig. 3h**). Brains from *Sod2* $^{+/-}$ haploinsufficient animals showed identical results. When endogenous oxidative stress was further elevated in bigenic (*prkn* $^{-/-}$*//Sod2* $^{+/-}$) animals, the same change in redox indices were detected (**Fig. 3h**), as measured in human parkin-deficient cells and cortices (above). These results established a functional relation between parkin protein expression, glutathione redox state and the degree of oxidative stress *in vivo*. We next studied potential mechanism(s) to explain the rise in GSH in the absence of parkin.

***De novo* synthesis of glutathione is not altered in parkin-deficient brain**

We first examined GSH *de novo* synthesis. When we measured the total pool of glutathione (GSH and GSSG) by HPLC in our parkin-deficient *vs.* WT parkin expression paradigms, we saw no differences for the total concentration across cell cultures, murine brains and human cortices (**Extended Data Fig. 4a, b, c**). In accordance, we found no difference in transcript numbers for the two rate-limiting enzymes in GSH synthesis, *i.e.*, the glutamate-cysteine-ligase-catalytic (*GCLC*) and glutamate-cysteine-ligase-modifier (*GCLM*) subunits [29], or for *Dj-1*, in mouse brain (**Extended Data Fig. 4d, e**).

Unexpectedly, in bigenic mice, where we recorded a significant rise in the total glutathione (GSH + GSSG) concentration ($P<0.05$), we also did not find higher copy numbers for *GCLC* or *GCLM* mRNA (**Extended Data Fig. 4c,e**). Thus, *de novo* synthesis from increased *GCLC* or *GCLM* gene transcription did not account for the glutathione redox changes seen in parkin's absence.

Glutathione recycling is altered in *prkn*-null brain

We next explored a second mechanism, namely the enhanced regeneration of GSH by glutathione reductase (GR). This enzyme is activated by rising levels of ROS or its substrate (GSSG), and is inhibited by excess product levels, such as GSH or $NADP^+$ [30-32]. By using the Tietze method, which utilizes exogenous GR activity to indirectly measure GSH and GSSG levels, we reproduced the same significant changes, *i.e.*, GSH elevation ($P<0.01$), GSSG lowering ($P<0.01$) and the rise of the GSH:GSSG ratio, in *prkn* $^{-/-}$ mice as found in cells and human brain (**Fig. 4a** and **Fig. 3c-f**, respectively). These findings in mouse brain matched the published results by Itier et al.; they suggested that GR activity was indeed higher in parkin's absence. We reasoned that activation of endogenous GR was even more elevated in ARPD cortices than in *prkn* $^{-/-}$ brain, because GSH levels were higher in the former than the latter using the GR-independent HPLC method (**Fig. 3f-h**).

Parkin contributes to the pool of recycled glutathione

Based on the dynamic changes observed in the redox state of cells and tissues when parkin was not detectable, we examined whether it had any direct effects on thiol network changes, such as GSH recycling. We specifically asked whether parkin interacted with GSSG. We first tested this *in vitro* using recombinant proteins, both tagged and untagged, and eosin-labelled GSSG (referred to as Di-E-GSSG) (**Extended Data Figs. 2f, 4f**). We discovered that full-length, human r-parkin had concentration-dependent activity in reducing Di-E-GSSG to the fluorescence-emitting E-GSH (545 nm) (**Fig. 4b**). Of note, Di-E-GSSG itself is non-fluorescent due to quenching[33]. N-terminally truncated parkin comprising the IBR-RING2 domains (aa 327-465) and a C-terminal RING2 peptide (aa 425-465) also showed E-GSH-regenerating activity (**Extended Data Fig. 4f**; not shown). In contrast, the control protein-tag alone (*e.g.*, maltose-binding protein (MBP); ~50 kDa)

and incubation with E-GSH (*i.e.*, without any Di-E-GSSG present) showed no activity in this assay (**Fig. 4b**; data not shown).

Resulting from this biochemical reaction, the formation of E-S-glutathionylated parkin (referred to as parkin-SG-E) was confirmed by using MBP-tagged parkin proteins and non-reducing SDS/PAGE analyses exposed to UV light. We found that the ~90 kDa MBP-parkin-SG-E and the ~60 kDa MBP-IBR-RING2-SG-E proteins were only visible under UV light after the incubation of native proteins with Di-E-GSSG (*e.g.*, **Extended Data Fig. 4g**, lane 2 of left panel). Furthermore, the incubation of MBP-IBR-RING2-SG-E and MBP-parkin-SG-E with either DTT or a reconstituted glutaredoxin-1 or -2 (Grx1, Grx2) system[33] reversed the S-glutathionylation of parkin, confirming that oxidation in the form of disulphide-bond formation had occurred during the earlier reaction (**Extended Data Fig. 4g**; and data not shown). In accordance, parkin proteins without any -SG-E modification did not interact with Grx1, Grx2, or thioredoxin-1 (Trx1; not shown). We reasoned that parkin's ability to directly bind GSSG could therefore alter the GSH *vs.* GSSG redox state of cells and tissue.

To further test this, we incubated untagged r-parkin (1μM) with various, eosin-free [GSH]:[GSSG] ratios to a total of 10μM (**Fig. 4c**). After 15 min, we measured GSH concentrations with an enzymatic, GSH-specific assay that uses monochlorobimane and glutathione-S-transferase activity. Following its incubation with GSSG alone, we determined that under these conditions parkin was able to reduce up to 5 equivalents of GSSG to GSH (6.8μM GSH minus a baseline signal of 1.3μM for r-parkin alone; **Fig. 4c**). Therefore, for every recycled GSSG molecule one reduced GSH and one S-glutathionylated thiol on parkin had been generated. These findings demonstrated a direct biochemical effect by parkin onto its thiol-based redox environment.

We next sought to map specific S-glutathionylation sites on parkin using MBP-parkin-SG preparations by mass spectrometry, which was performed under non-reducing conditions. Full-length MBP-parkin-SG-E was subjected to trypsin digestion followed by LC-MS/MS and MALDI analyses. We detected two residues that were consistently S-glutathionylated, *i.e.*, the conserved cysteine 59 and human-specific cysteine 95; each

carried an extra mass of 305.0682 (**Fig. 4d, e**), corresponding to S-linked glutathionylated oxidation of parkin. A third, but less frequently identified residue that was S-glutathionylated was cysteine 377 within parkin's IBR domain. To date, we have not yet identified modified cysteine(s) in the untagged, C-terminal RING2 peptide, which also had shown GSSG-recycling activity. We concluded from these complementary results that S-glutathionylation represents a *bona fide* oxidative modification of parkin, which arises from its interaction with GSSG.

DISCUSSION

Our study generated four novel insights into the protective effects of PD-linked parkin: One, we restaged in cell models and mouse brain the age-associated loss of parkin solubility that occurs in human brain[11,20] by promoting its progressive oxidation using mitochondrial and cytosolic stressors (**Fig. 1; Extended Data Fig. 1**). We then monitored for specific cysteine oxidation sites in murine parkin using LC-MS/MS (**Extended Data Fig. 2f, g; Extended Data Table 1**). There, we found a relative loss of free thiols in parkin associated with the rise of oxidative stress in MPTP-treated mice. We also mapped several cysteines that had undergone irreversible oxidation events, such as to sulfinic and sulfonic acid, under both basal and oxidizing conditions, *e.g.*, C211, C195, C237, C252, and C376 (**Extended Data Table 1**). We noticed with interest –given the role of parkin phosphorylation by ARPD-linked PINK1 during mitophagy[34]- that S77 of murine parkin was found to be phosphorylated in MPTP stress-exposed brain (**Extended Data Table 1**).

Two, we established that *PRKN* expression contributes to cytosolic ROS neutralization and *in vivo* redox homeostasis; this, to limit oxidative stress in high energy-demanding organs, such as the brain (shown here) and heart (El-Kodsi et al., in preparation). Its role in ROS neutralization complements parallel studies that centred on neuronal parkin's role in dopamine oxidation-related stress[11]. This anti-oxidant effect is mediated by parkin's cysteines, which are sensitive to both oxidizing and reducing environments (**Fig. 2a; Extended Data Fig.2a-g**). We found that parkin's effect on redox homeostasis leads to

downstream protection from chronic oxidative stress, seen in the lower carbonyl content in mouse and human tissues (**Fig. 2f-i**), as first described by Palacino et al.[15]. We also provided evidence that parkin's modulation of cytosolic ROS is linked to downstream effects on redox-sensitive, mitochondrial enzymatic activities (*e.g.*, Aco2, **Fig. 2j**), which were previously found altered but mechanistically unexplained in parkin-deficient mice by Periquet et al.[16]. Linking parkin's role in mitigating ROS concentrations in the cytosol to mitochondrial activity also helps explain the prediction made by Berger et al., who had postulated an 'intrinsic, pro-mitochondrial effect by parkin'[35]. We suspect that the structural changes in redox-sensitive proteins from *prkn*$^{-/-}$ mice[15,16] were mediated by the net reduction in free cellular thiols, thereby conferring less protection from endogenously generated oxidative stress (**Figs. 2, 3).** Our results therefore link parkin's own oxidation to concrete redox benefits in cells and *in vivo,* thus supporting the notion that parkin is a 'multipotent, protective protein'[36].

Three, parkin's cellular protection from ROS appeared independent of E3 ligase activity. Its oxidation had previously been widely interpreted as a loss of its E3 ligase activity[37,38], Here, we demonstrated that parkin confers cellular protection and ROS mitigation while being subjected to oxidizing conditions that would have abrogated its E3 ligase activity[10]. We also determined that HMW forms of WT parkin, which were produced during oxidizing conditions, collapsed when treated with DTT; this reversal would not occur for parkin species formed by auto-polyubiquitination[39]. These findings could theoretically suggest that E3 ligase function is not essential to parkin's oxidative stress-mitigating role. However, parkin's redox-regulating activity may not be mutually exclusive from its ubiquitin ligase activity. It is known that low levels of oxidation can activate E3 ligase function *ex vivo*; moreover, both cellular redox-regulation and E3 ligase activity require thiol-based chemistry[10,37,40,41]. In support of a low level of parkin activation, we noted that it is oxidized under basal conditions in both murine (**Extended Data Table 1**) and human brain[11]. Furthermore, the reversible nature of some (but not all) of these oxidative modifications suggests that parkin continuously undergoes oxidative events *in vivo*. Therefore, we propose that distinct cellular conditions may rely more on parkin's redox functions, such as during elevated oxidative stress, whereas others rely more on its E3

activity, such as in baseline protein homeostasis and organelle-specific autophagy. Importantly, because powerful oxidative stressors are required to recapitulate in mice parkin's aggregation and insolubility (**Fig. 1**), which occurs physiologically in aged control brain[11], we speculate that parkin is cumulatively exposed to highly oxidizing conditions in long-lived humans.

Four, we uncovered a reciprocal relationship between glutathione's redox state and *PRKN* expression *in vivo*, and generated evidence that parkin plays a direct role in GSSG recycling. The thiol network, to which we propose parkin contributes, is critical in the maintenance of overall redox balance, and thus, to cellular and organ health[42,43]. Here, we expand on the initial observation made by Itier et al. of a GSH elevation in young *prkn*$^{-/-}$ mice[27] by comparing a variety of cellular and mouse models to human brain (**Fig. 3**). In parkin's absence: i) GSH is elevated to increase the total number of free thiols; ii) GSSG levels are diminished; iii) the ratio of GSH:GSSG is increased; and iv) total glutathione levels (GSH + GSSG) are unchanged, except in bigenic mice (**Fig. 3c-f, h; Extended Data Fig. 4a-c, e**). We postulate that parkin's presence reduced cellular needs for higher levels of free GSH. We first explored *de novo* synthesis of GSH but found no increase in *GCLM* or *GCLC* mRNA levels. As for the rise in total glutathione in bigenic mice, we reasoned that higher GSH levels may still have resulted from increased synthesis but via more effective translation of already existing *GCLM* mRNA[29,32], or elevated enzymatic activity, rather than *de novo* gene transcription. Comparing HPLC *vs.* the GR-based Tietze method in murine brain, we observed an increase in GSH levels and reciprocal decrease in GSSG levels in *prkn*$^{-/-}$ mice when using the latter method, which was therefore attributable to an increase in GR enzyme-related activity (**Fig. 4a, f**)[31,32]. Because we had observed dynamic changes in GSSG levels in cell models following increased parkin expression and oxidative stress (**Fig. 3c-e**), we next explored if parkin contributed to increased GSH levels by direct thiol-mediated recycling of GSSG. There, we found that parkin directly bound to GSSG in a concentration-dependent manner, which resulted in half of GSSG recycled to GSH and the other half attached to parkin via S-glutathionylation (**Fig. 4b-e**).

The finding of parkin S-glutathionylation (**Fig. 4b, c**), and its reversal by glutaredoxin-1 and -2, further highlights the relevance of parkin's integration into redox chemistry. The oxidation of proteins via S-glutathionylation represents a major contributor to redox signaling and generally serves as a protective mechanism.[44,45] We noted with interest that primate-specific cysteine 95 is targeted for oxidation by both S-glutathionylation (**Fig. 4e**) and dopamine radical adduct formation[11]. We question whether this specific residue, which is located in the linker region of human parkin, could have an effect on parkin activation akin to S65 phosphorylation during mitophagy. We anticipate that the many posttranslational modifications of parkin, which we have unequivocally identified here by LC-MS/MS, will inform structurally oriented and cell biological research in the future. Such investigations, which may focus on the linker region[34] and downstream mitochondrial health[46] , should be explored in the context of parkin's redox chemistry. Due to the inherently transient nature of S-glutathionylation (as well as of S-nitrosylation[40]) as a posttranslational modification and due to the analytical methods used to map cysteine modifications in murine (**Extended Data Table 1**) and human brain in our work[11], namely under alkylating and reducing conditions, we have not yet validated parkin S-glutathionylation *in vivo*. We hope to continue these investigations in the near future.

Future studies will also explore which region and which cell type in the nervous system[28] contribute most significantly to the parkin-dependent glutathione redox changes we have observed *in vivo*. The lack of significantly increased GSH levels in *prkn*$^{-/-}$ mouse brain by HPLC methodology suggests that these animals can compensate for increased cytosolic ROS via other redox state-regulating mechanisms, such as via glutathione peroxidase (GPx) activity (**Fig. 4f**). High tolerance to ROS may help explain the lack of a parkinsonian phenotype in *prkn*-null mice[19,27,47]. In aged mouse brain, an additional stressor could be required, such as demonstrated in our bigenic (*prkn*$^{-/-}$//*Sod2*$^{+/-}$) mice. Of note, a human-specific redox aspect is that in long-lived primates nigral neurons experience higher ROS levels, dysregulated iron homeostasis, and radicals from oxidative dopamine metabolism[11,48,49]. Differences in human *vs.* murine parkin oxidative metabolism will thus be further explored.

The strengths of our investigations are three-fold: 1) results in cellular and murine models restaged findings in human tissues[11,20] (**Figs. 2h, i; 3f, g**); 2) our research integrated *in vitro*, *ex vivo* and *in vivo* paradigms as well as exogenous and endogenous ROS sources; and 3) the redox hypothesis of parkin's function readily explains its many reported roles in distinct cellular paradigms, *e.g.*, cancer biology, mitochondrial health, immunity, etc.[50], because these pathways are (co-)regulated by redox state changes (**Fig. 4f**).

We have also identified shortcomings. First, in future work we will conduct a more extensive assessment of the diversity and quantity of oxidative modifications in brain parkin by LC-MS/MS, for example in our MPTP-exposed *vs.* untreated mouse model, in order to map additional *bona fide* oxidation sites that occur *in vivo*. As mentioned, we have yet to validate S-glutathionylation of parkin *in vivo*, which will require optimization of mass spectrometry techniques. Furthermore, we wish to study a greater number of *PRKN*-genotyped, age-matched, human brain specimens to quantify protein carbonylation and nitrotyrosination, as well as to explore human brain-specific changes in redox state-related transcriptomes from different areas of the brain. Recently, we have begun to characterize glutathione-regulating enzyme levels *in vivo*, *e.g.*, glutathione-reductase, to validate our model that its activity is markedly increased in ARPD (**Fig. 4f**).

Our discovery that parkin's seemingly diverse activities are anchored in traditional redox chemistry (**Fig. 4f**) provides at once a biochemical and a unifying explanation for its role in neuroprotection. It may also help answer the two decades-old question: "What function of parkin is essential in conferring the selective protection of dopamine neurons in the adult human brainstem?"[11,51] Further exploration of parkin's redox effects should create new opportunities for urgently needed therapies for patients with young-onset, currently incurable parkinsonism.

REFERENCES

1 Takahashi, H. *et al.* Familial juvenile parkinsonism: clinical and pathologic study in a family. *Neurology* **44**, 437-441, doi:10.1212/wnl.44.3_part_1.437 (1994).

2 Mori, H. *et al.* Pathologic and biochemical studies of juvenile parkinsonism linked to chromosome 6q. *Neurology* **51**, 890-892, doi:10.1212/wnl.51.3.890 (1998).

3 Zecca, L. *et al.* The role of iron and copper molecules in the neuronal vulnerability of locus coeruleus and substantia nigra during aging. *Proc Natl Acad Sci U S A* **101**, 9843-9848, doi:10.1073/pnas.0403495101 (2004).

4 Pacelli, C. *et al.* Elevated Mitochondrial Bioenergetics and Axonal Arborization Size Are Key Contributors to the Vulnerability of Dopamine Neurons. *Curr Biol* **25**, 2349-2360, doi:10.1016/j.cub.2015.07.050 (2015).

5 Giguere, N., Burke Nanni, S. & Trudeau, L. E. On Cell Loss and Selective Vulnerability of Neuronal Populations in Parkinson's Disease. *Front Neurol* **9**, 455, doi:10.3389/fneur.2018.00455 (2018).

6 Burbulla, L. F. *et al.* Dopamine oxidation mediates mitochondrial and lysosomal dysfunction in Parkinson's disease. *Science* **357**, 1255-1261, doi:10.1126/science.aam9080 (2017).

7 Shimura, H. *et al.* Familial Parkinson disease gene product, parkin, is a ubiquitin-protein ligase. *Nat Genet* **25**, 302-305, doi:10.1038/77060 (2000).

8 Matsuda, N. *et al.* PINK1 stabilized by mitochondrial depolarization recruits Parkin to damaged mitochondria and activates latent Parkin for mitophagy. *J Cell Biol* **189**, 211-221, doi:10.1083/jcb.200910140 (2010).

9 Narendra, D., Tanaka, A., Suen, D. F. & Youle, R. J. Parkin is recruited selectively to impaired mitochondria and promotes their autophagy. *J Cell Biol* **183**, 795-803, doi:10.1083/jcb.200809125 (2008).

10 LaVoie, M. J., Ostaszewski, B. L., Weihofen, A., Schlossmacher, M. G. & Selkoe, D. J. Dopamine covalently modifies and functionally inactivates parkin. *Nat Med* **11**, 1214-1221, doi:10.1038/nm1314 (2005).

11 Tokarew, J. M. *et al.* Oxidative Modifications of Parkin Underlie its Selective Neuroprotection in Adult Human Brain. *bioRxiv*, 2020.2002.2019.953034, doi:10.1101/2020.02.19.953034 (2020).

12 Schapira, A. H. & Gegg, M. Mitochondrial contribution to Parkinson's disease pathogenesis. *Parkinsons Dis* **2011**, 159160, doi:10.4061/2011/159160 (2011).

13 Martinez, T. N. & Greenamyre, J. T. Toxin models of mitochondrial dysfunction in Parkinson's disease. *Antioxid Redox Signal* **16**, 920-934, doi:10.1089/ars.2011.4033 (2012).

14 Townsend, D. M., Tew, K. D. & Tapiero, H. The importance of glutathione in human disease. *Biomed Pharmacother* **57**, 145-155, doi:10.1016/s0753-3322(03)00043-x (2003).

15 Palacino, J. J. *et al.* Mitochondrial dysfunction and oxidative damage in parkin-deficient mice. *J Biol Chem* **279**, 18614-18622, doi:10.1074/jbc.M401135200 (2004).

16 Periquet, M., Corti, O., Jacquier, S. & Brice, A. Proteomic analysis of parkin knockout mice: alterations in energy metabolism, protein handling and synaptic function. *J Neurochem* **95**, 1259-1276, doi:10.1111/j.1471-4159.2005.03442.x (2005).

17 LaVoie, M. J., Cortese, G. P., Ostaszewski, B. L. & Schlossmacher, M. G. The effects of oxidative stress on parkin and other E3 ligases. *J Neurochem* **103**, 2354-2368, doi:10.1111/j.1471-4159.2007.04911.x (2007).

18 Andres-Mateos, E. *et al.* DJ-1 gene deletion reveals that DJ-1 is an atypical peroxiredoxin-like peroxidase. *Proc Natl Acad Sci U S A* **104**, 14807-14812, doi:10.1073/pnas.0703219104 (2007).

19 Goldberg, M. S. *et al.* Parkin-deficient mice exhibit nigrostriatal deficits but not loss of dopaminergic neurons. *J Biol Chem* **278**, 43628-43635, doi:10.1074/jbc.M308947200 (2003).

20 Pawlyk, A. C. *et al.* Novel monoclonal antibodies demonstrate biochemical variation of brain parkin with age. *J Biol Chem* **278**, 48120-48128, doi:10.1074/jbc.M306889200 (2003).

21 Ali, S. F., David, S. N., Newport, G. D., Cadet, J. L. & Slikker, W., Jr. MPTP-induced oxidative stress and neurotoxicity are age-dependent: evidence from measures of reactive oxygen species and striatal dopamine levels. *Synapse* **18**, 27-34, doi:10.1002/syn.890180105 (1994).

22 Hinerfeld, D. *et al.* Endogenous mitochondrial oxidative stress: neurodegeneration, proteomic analysis, specific respiratory chain defects, and efficacious antioxidant therapy in superoxide dismutase 2 null mice. *J Neurochem* **88**, 657-667, doi:10.1046/j.1471-4159.2003.02195.x (2004).

23 Spratt, D. E. *et al.* A molecular explanation for the recessive nature of parkin-linked Parkinson's disease. *Nat Commun* **4**, 1983, doi:10.1038/ncomms2983 (2013).

24 Han, D., Antunes, F., Canali, R., Rettori, D. & Cadenas, E. Voltage-dependent anion channels control the release of the superoxide anion from mitochondria to cytosol. *J Biol Chem* **278**, 5557-5563, doi:10.1074/jbc.M210269200 (2003).

25 Shimura, H. *et al.* Ubiquitination of a new form of alpha-synuclein by parkin from human brain: implications for Parkinson's disease. *Science* **293**, 263-269, doi:10.1126/science.1060627 (2001).

26 Wiese, A. G., Pacifici, R. E. & Davies, K. J. Transient adaptation of oxidative stress in mammalian cells. *Arch Biochem Biophys* **318**, 231-240, doi:10.1006/abbi.1995.1225 (1995).

27 Itier, J. M. *et al.* Parkin gene inactivation alters behaviour and dopamine neurotransmission in the mouse. *Hum Mol Genet* **12**, 2277-2291, doi:10.1093/hmg/ddg239 (2003).

28 Solano, R. M. *et al.* Glial dysfunction in parkin null mice: effects of aging. *J Neurosci* **28**, 598-611, doi:10.1523/JNEUROSCI.4609-07.2008 (2008).

29 Sikalidis, A. K. *et al.* Upregulation of capacity for glutathione synthesis in response to amino acid deprivation: regulation of glutamate-cysteine ligase subunits. *Amino Acids* **46**, 1285-1296, doi:10.1007/s00726-014-1687-1 (2014).

30 Tietze, F. Enzymic method for quantitative determination of nanogram amounts of total and oxidized glutathione: applications to mammalian blood and other tissues. *Anal Biochem* **27**, 502-522, doi:10.1016/0003-2697(69)90064-5 (1969).

31 Frasier, C. R. *et al.* Redox-dependent increases in glutathione reductase and exercise preconditioning: role of NADPH oxidase and mitochondria. *Cardiovasc Res* **98**, 47-55, doi:10.1093/cvr/cvt009 (2013).

32 Espinosa-Diez, C. *et al.* Antioxidant responses and cellular adjustments to oxidative stress. *Redox Biol* **6**, 183-197, doi:10.1016/j.redox.2015.07.008 (2015).

33 Sengupta, R., Coppo, L., Mishra, P. & Holmgren, A. Glutathione-glutaredoxin is an efficient electron donor system for mammalian p53R2-R1-dependent ribonucleotide reductase. *J Biol Chem* **294**, 12708-12716, doi:10.1074/jbc.RA119.008752 (2019).

34 Aguirre, J. D., Dunkerley, K. M., Mercier, P. & Shaw, G. S. Structure of phosphorylated UBL domain and insights into PINK1-orchestrated parkin activation. *Proc Natl Acad Sci U S A* **114**, 298-303, doi:10.1073/pnas.1613040114 (2017).

35 Berger, A. K. *et al.* Parkin selectively alters the intrinsic threshold for mitochondrial cytochrome c release. *Hum Mol Genet* **18**, 4317-4328, doi:10.1093/hmg/ddp384 (2009).

36 Feany, M. B. & Pallanck, L. J. Parkin: a multipurpose neuroprotective agent? *Neuron* **38**, 13-16 (2003).

37 Chung, K. K. *et al.* S-nitrosylation of parkin regulates ubiquitination and compromises parkin's protective function. *Science* **304**, 1328-1331, doi:10.1126/science.1093891 (2004).

38 Meng, F. *et al.* Oxidation of the cysteine-rich regions of parkin perturbs its E3 ligase activity and contributes to protein aggregation. *Mol Neurodegener* **6**, 34, doi:10.1186/1750-1326-6-34 (2011).

39 Komander, D. The emerging complexity of protein ubiquitination. *Biochem Soc Trans* **37**, 937-953, doi:10.1042/BST0370937 (2009).

40 Yao, D. *et al.* Nitrosative stress linked to sporadic Parkinson's disease: S-nitrosylation of parkin regulates its E3 ubiquitin ligase activity. *Proc Natl Acad Sci U S A* **101**, 10810-10814, doi:10.1073/pnas.0404161101 (2004).

41 Vandiver, M. S. *et al.* Sulfhydration mediates neuroprotective actions of parkin. *Nat Commun* **4**, 1626, doi:10.1038/ncomms2623 (2013).

42 Go, Y. M. & Jones, D. P. The redox proteome. *J Biol Chem* **288**, 26512-26520, doi:10.1074/jbc.R113.464131 (2013).

43 Go, Y. M., Chandler, J. D. & Jones, D. P. The cysteine proteome. *Free Radic Biol Med* **84**, 227-245, doi:10.1016/j.freeradbiomed.2015.03.022 (2015).

44 Xiong, Y., Uys, J. D., Tew, K. D. & Townsend, D. M. S-glutathionylation: from molecular mechanisms to health outcomes. *Antioxid Redox Signal* **15**, 233-270, doi:10.1089/ars.2010.3540 (2011).

45 Sabens Liedhegner, E. A., Gao, X. H. & Mieyal, J. J. Mechanisms of altered redox regulation in neurodegenerative diseases--focus on S--glutathionylation. *Antioxid Redox Signal* **16**, 543-566, doi:10.1089/ars.2011.4119 (2012).

46 Koyano, F. *et al.* Ubiquitin is phosphorylated by PINK1 to activate parkin. *Nature* **510**, 162-166, doi:10.1038/nature13392 (2014).
47 Kitada, T. *et al.* Impaired dopamine release and synaptic plasticity in the striatum of parkin-/- mice. *J Neurochem* **110**, 613-621, doi:10.1111/j.1471-4159.2009.06152.x (2009).
48 Zucca, F. A. *et al.* Neuromelanin organelles are specialized autolysosomes that accumulate undegraded proteins and lipids in aging human brain and are likely involved in Parkinson's disease. *NPJ Parkinsons Dis* **4**, 17, doi:10.1038/s41531-018-0050-8 (2018).
49 Zucca, F. A. *et al.* Interactions of iron, dopamine and neuromelanin pathways in brain aging and Parkinson's disease. *Prog Neurobiol* **155**, 96-119, doi:10.1016/j.pneurobio.2015.09.012 (2017).
50 Xu, L., Lin, D. C., Yin, D. & Koeffler, H. P. An emerging role of PARK2 in cancer. *J Mol Med (Berl)* **92**, 31-42, doi:10.1007/s00109-013-1107-0 (2014).
51 Kitada, T. *et al.* Mutations in the parkin gene cause autosomal recessive juvenile parkinsonism. *Nature* **392**, 605-608, doi:10.1038/33416 (1998).
52 Hu, J. & Li, S. Electroporation formulation for cell therapy. *Methods Mol Biol* **1121**, 55-60, doi:10.1007/978-1-4614-9632-8_4 (2014).
53 Kumar, A. *et al.* Disruption of the autoinhibited state primes the E3 ligase parkin for activation and catalysis. *EMBO J* **34**, 2506-2521, doi:10.15252/embj.201592337 (2015).
54 Matsuda, N. *et al.* Diverse effects of pathogenic mutations of Parkin that catalyze multiple monoubiquitylation in vitro. *J Biol Chem* **281**, 3204-3209, doi:10.1074/jbc.M510393200 (2006).
55 Rahman, I., Kode, A. & Biswas, S. K. Assay for quantitative determination of glutathione and glutathione disulfide levels using enzymatic recycling method. *Nat Protoc* **1**, 3159-3165, doi:10.1038/nprot.2006.378 (2006).
56 Casagrande, S. *et al.* Glutathionylation of human thioredoxin: a possible crosstalk between the glutathione and thioredoxin systems. *Proc Natl Acad Sci U S A* **99**, 9745-9749, doi:10.1073/pnas.152168599 (2002).
57 Diaz, D. *et al.* Tissue specific changes in the expression of glutamate-cysteine ligase mRNAs in mice exposed to methylmercury. *Toxicol Lett* **122**, 119-129, doi:10.1016/s0378-4274(01)00341-1 (2001).
58 Shi, S. Y. *et al.* DJ-1 links muscle ROS production with metabolic reprogramming and systemic energy homeostasis in mice. *Nat Commun* **6**, 7415, doi:10.1038/ncomms8415 (2015).
59 Abelev, B. I. *et al.* Longitudinal double-spin asymmetry and cross section for inclusive jet production in polarized proton collisions at square root of s = 200 GeV. *Phys Rev Lett* **97**, 252001 (2006).

MATERIALS AND METHODS

Mouse tissues

Brains and hearts were collected from wild-type C57Bl/6J from Jackson laboratories, *prkn*-null from Dr. Brice's laboratory [27], *Sod2* +/- mice from Jackson laboratories; the bigenic mouse (*prkn*$^{-/-}$//*Sod2*$^{+/-}$) was created by crossing *prkn*-null mice with *Sod2* haploinsufficient mice, and interbreeding heterozygous offspring. The bigenic mouse will be further characterized elsewhere (El Kodsi et al., in preparation). Mouse brains collected were homogenized on ice in a Dounce glass homogenizer by 20 passes in Tris salt buffer with or without the addition of 1% H_2O_2, transferred to ultracentrifuge tubes and spun at 55,000 and 4°C for 30 mins to extract the soluble fraction. The resulting pellets were further homogenized in the tris salt buffer with the addition of 2-10% SDS, transferred to ultracentrifuge tubes and spun at 55,000 rpm and 10°C for 30 minutes to extract the insoluble fraction.

Cell culture, transfection and oxidation

Human embryonic kidney (HEK-293) were grown in Dulbecco's Modified Eagle Medium (DMEM) supplemented with 1 % penicillin/streptomycin and 10 % heat-inactivated fetal bovine serum (FBS) at 37°C with 5 % CO_2. Four to 15 μg of cDNA coding for N-terminally flag-tagged parkin or empty Flag control vector (pcDNA3.1+) using a 1:1 ratio of cDNA:Lipofectamine 2000, was used for ectopic overexpression. The cDNA and Lipofectamine 2000 were incubated for 20 min at room temperature before being applied directly to the cells for 1 hour at 37°C with 5 % CO_2 followed by direct addition of fresh growth medium. Cells were incubated another 24 hours before treatment, harvesting and analysis. Control Chinese hamster ovary cells, stably expressing the myc-vector (CHO), or expressing myc-parkin (CHOmP) were also used.

All chemicals (H_2O_2, CCCP, NEM, IAA, DTT, AT, BSO and NAC) were added directly to cells at ~75% confluence in growth media or OPTI-MEM media. Cells were manually scrapped, spun at a 1000 rpm for 5 minutes, the pellets washed with PBS and then

homogenized in a Tris salt buffer, transferred to ultracentrifuge tubes and spun at 55,000 rpm and 4°C for 30 minutes to extract the soluble fraction. The resulting pellets were further homogenized in the Tris salt buffer with the addition of 2-10% SDS, transferred to ultracentrifuge tubes and spun at 55,000 rpm and 10°C for 30 minutes to extract the insoluble fraction. SH-SY5Y cells were generally seeded at a density of 0.5-1 x 106 cells/mL. Once cells reached 70-80 % confluency they were transfected with cDNA coding for C-terminally Flag-tagged Parkin or empty Flag control vector (pcDNA3) by electroporation using the nucleofector method described by Hu and Li, 2015. A total of 2 million cells were resuspended in 100 µL of OPTI-MEM containing cDNA (2 µg) and 1 % polyoxamer 188. The cells were electroporated using the X Unit and pulse code "CA-137" on a Lonza 4D-Nucleofector. Following electroporation, cells were seeded at a concentration of 0.8-1 x 106 cells/mL [52].

Western blot and densitometry

Brain homogenates and cell lysates were run on 4-12 % Bis-Tris SDS-PAGE gels using MES running buffer. Proteins were transferred to PVDF membranes using transfer buffer, and immunoblotted for parkin, DJ-1, MnSOD, aconitase-2, nitrotyrosine, flag- and myc-tag epitopes. Actin and Ponceau S staining were used as loading controls. For densitometry quantification, the signal intensity of parkin from each sample was measured as pixel using Image J Software, and controlled for loading, against actin's band intensity. Proteins were also stained in gel using Coomassie brilliant blue R-250 dye. The gel was first fixed in 10% acetic acid, 50% methanol, followed by staining for 2-24 hours with Coomassie and finally destained in 7.5% acetic acid, 5% methanol until crisp blue bands appeared.

MPTP treatment

Eight to 12 months old WT and *prkn*-null mice were injected intraperitoneally with 40mg/kg of saline or MPTP and sacrificed an hour later [21]. The brains were harvested for ROS measurement, protein analysis by Western blot and immunoprecipitation of parkin and mass spectrometry analysis. For mass spectrometry, the brains harvested were first

incubated in IAA prior to homogenization and fractionation as described above. Brain homogenates were then incubated with anti-parkin conjugated to magnetic beads (Dynabeads Coupling Kit; Invitrogen). A magnet was used to capture parkin bound to the beads, and several washes were used to remove unbound proteins. Eluted fractions (IP elute) along with controls (input, unbound, wash and recombinant parkin protein standards) were run on SDS/PAGE and blotted with anti-parkin. A sister gel was stained with Coomassie as described above and gel slices corresponding to band sizes 50-75 kDa were excised and analyzed by LC-MS/MS, as described in detail by Tokarew et al., 2020.

Recombinant, tag-less protein expression in pET-SUMO vector

Wild-type and truncated (residues 321-465) human parkin were expressed as 6His-Smt3 fusion proteins in *Escherichia coli* BL21 (DE3) Codon-Plus RIL competent cells (C2527, New England Biolabs) as previous described[23,34,53]. DJ-1 and SNCA coding sequences were cloned from a pcDNA3.1 vector into the pET-SUMO vector using PCR and restriction enzymes. All proteins were overexpressed in *E. coli* BL21 Codon-Plus competent cells (C2527, New England Biolabs) and grown at 37 °C in 2 % Luria Broth containing 30 mg/L kanamycin until OD600 reached 0.6, at which point the temperature was reduced to 16°C. Parkin protein-expressing cultures were also supplemented with 0.5 mM $ZnCl_2$. Once OD600 reached 0.8, protein expression was induced with isopropyl β-D-1-thiogalactopyranoside, except ulp1 protease, which was induced once OD600 had reached 1.2. The concentration of IPTG used for each construct is as follows: 25 μM for wild-type and point mutants of parkin, and 0.75 mM for truncated parkin, DJ-1, α-synuclein, SAG, and ulp1 protease. Cultures were left to express protein for 16-20 h. Cells were then harvested, centrifuged, lysed and collected on Ni-NTA agarose beads in elution columns.

Recombinant maltose-binding protein-tagged protein expression in pMAL-2T vector

Wild-type and truncated (residues 327-465) human parkin were expressed in the pMAL-2T vector (a gift from Dr. Keiji Tanaka), as previously described[54]. Parkin produced in this vector contained an N-terminal maltose-binding protein (MBP) and thrombin cleavage site (LVPRGS). All proteins were overexpressed in *E. coli* BL21 Codon-Plus competent cells (C2527, New England Biolabs) and grown at 37 °C in 2 % Luria Broth containing 0.2 % glucose and 100 mg/L ampicillin until OD600 reached 0.3-0.37, at which point protein expression was induced with addition of 0.4 mM isopropyl β-D-1-thiogalactopyranoside. Cultures were left to express protein at 37 °C until OD600 reached 0.9-1.0. Harvested protein isolates were purified using amylose resin in buffers containing 100 μM zinc sulfate and 10 mM maltose.

ROS (H_2O_2) measurements of recombinant proteins, tissue and cell lysates

Amplex® Red hydrogen peroxide/peroxidase assay kit (Invitrogen A22188) was used to monitor endogenous levels of H_2O_2 in tissues and cells, and residual levels of H_2O_2 after incubation with recombinant parkin (WT, or pre-incubated with increasing concentrations of H_2O_2, NEM, or EDTA), DJ-1, SNCA, BSA, RNF43 (from BioLegend), HOIP (from Boston Biochem), GSH, catalase, NEM and EDTA for 30 minutes. Pre-weighed cortex pieces from human brains (or pelleted cells) were homogenized on ice in the 1x reaction buffer provided, using a Dounce homogenizer (3 times volume to weight ratio). Homogenates were diluted in the same 1x reaction buffer (10x and 5x). A serial dilution of the H_2O_2 standard provided was prepared (20, 10, 2 and 0 μM). 50 μL of standards and samples were plated in a 96 well black plate with clear flat bottom. The reaction was started by the addition of 50μL working solution which consist of 1x reaction buffer, Amplex® red and horseradish peroxidase. The plate was incubated at room temperature for 30 minutes protected from light. A microplate reader was used to measure either fluorescence with excitation at 560 nm and emission at 590 nm, or absorbance at 560 nm. The obtained H_2O_2 levels (μM) were normalized to the tissue

weight (g) or protein concentration (µg/µL). The same aasay was also used to measure parkin and glutathione's peroxides activity compared to horseradish peroxidase (HRP).

ROS (H_2O_2) measurements of intact cells

HEK 293 cells were transfected with flag-parkin or control vector (pcDNA) as described above. After 24 h the cells were lifted using trypsin and re-seeded in a 12-well dish at a density of 0.3 x 106 cells/mL. After 48 h the cells were treated with 0 mM or 2 mM H_2O_2 in OPTI-MEM medium at 37°C and 5 % CO_2. After 1 h the cells were washed with OPTI-MEM and incubated with 20 µM of dichlorofluorescin diacetate (DCFH-DA, D6883, Sigma) for 30 min at 37°C and 5 % CO_2. Cells were collected using a cell lifter and treated with ethidium-1 dead stain (E1169, Invitrogen) for 15 min at room temperature. Samples were analyzed using a BD Fortessa flow cytometer set to measure the ROS-sensitive probe (DCFH-DA, ex. 488 nm and em. 527 nm) and viability stain (ethidium-1, ex, 528 nm and em. 617 nm). The results were reported as the average mean fluorescence intensity (MFI) of ROS in live cells. Each separate transfection was considered one biological replicate.

Cell cytotoxicity assay

Vybrant ™ cytotoxicity assay kit (Molecular Probes V-23111) was used to monitor cell death through the release of the cytosolic enzyme glucose 6-phosphate dehydrogenase (G6yPD) from damaged cells into the surrounding medium. 50 µl of media alone (no cells), media from control and stressed VHO and CHOmP cells and cell lysates were added to a 96-well microplate. 50 µl of reaction mixture, containing reaction buffer, reaction mixture and resazurin, was added to all wells, and the mircroplate was incubated at 37°C for 30 mins. A microplate reader was used to measure either fluorescence with excitation at 560 nm and emission at 590 nm. A rise in fluoresence indicates a rise in G6PD levels i.e. a rise in cell death.

GSH and GSSG quantification - HPLC

Human and mouse brain pieces, and CHO cell pellets were homogenized in a buffer containing 125 mM sucrose, 5 mM TRIS, 1.5 mM EDTA, 0.5%TFA and 0.5%MPA in mobile phase. Then samples were spun at 14000xg at 4 °C for 20 min. Supernatants were collected and analyzed using an Agilent HPLC system equipped with a Pursuit C_{18} column (150 ×4.6 mm, 5 µm; Agilent Technologies) operating at a flow rate of 1 ml/min or. The mobile phase consisted of 0.09% trifluoroacetic acid diluted in ddH2O and mixed with HPLC-grade methanol in a 90:10 ratio. Standard solutions were used to estimate the retention times for GSH and GSSG. Using Agilent Chemstation software, absolute amounts of GSH and GSSG were acquired by integrating the area under the corresponding peaks, and values were calculated from standard curves

GSH concentration determination by monochlorobimane assay

Stock solutions of assay dye (monochlorobimane (mcB), 22 mM) and glutathione-S-transferase (50 units/mL) were prepared in PBS and stored protected from light at -20°C. The working solution was prepared using 12.8 µL of stock mcB and 80 µL of stock glutathione-S-transferase in 4 mL PBS and stored on ice. Samples were prepared as follows: cells were lifted mechanically using cell-lifters, washed twice and re-suspended in ice-cold PBS, mixed by vortex and incubated on ice for 30 min. Following two freeze thaw cycles using solid CO_2, the samples were sonicated 1 min on wet ice (S220 Ultra-sonicator from Covaris) and spun at 3000 x g, 4°C, for 5 min. Total protein concentration of supernatants was determined using Bradford assay. Samples and glutathione (GSH) standards (0- 13 µM) were plated in 25 µL aliquots in a 96-well plate with clear bottom and black sides. 25 µL of working solution was added to all experimental wells and protected from light for 15 min at room temperature. Fluorescence (ex 380 nm, em 461 nm) was measured using a Synergy H1Multi-Mode Plate Reader (Bio Tek). The amount of GSH detected in each sample was calculated using the regression curve obtained from the glutathione standards.

Tietze's enzymatic recycling determination of GSH and GSSG

The enzymatic recycling method described by Rahman et al. [55] was used to determine reduced glutathione (GSH) and oxidized glutathione (GSSG) levels in mouse brain lysates. Hemi-brains of wild type (n=3) and parkin KO (n=3) mice, at 13 and 11 months of age respectively, were collected, weighed and homogenized in 3X volume/weight of KPEX (0.1 M potassium phosphate, 5 mM EDTA, 0.1 % Triton X-100, 0.6 % sulfosalicylic acid, pH 7.5) using a glass Dounce homogenizer (50 passes). Samples were spun at 8000 x g, 4°C, for 5 min and the supernatant protein concentration was determined using Bradford assay. To determine the total glutathione (GSH + GSSG) concentration, the following stock solutions were freshly prepared in KPE (0.1 M potassium phosphate, 5 mM EDTA, pH 7.5): 5,5'-dithio-bis-[2-nitrobenzoic acid] (DNTB) at 0.6 mg/mL, nicotinamide adenine dinucleotide phosphate (NADPH) at 0.6 mg/mL and glutathione reductase at 3 units/mL. GSH standards were prepared in KPE at concentrations of 0-26 nM/mL. 20 µL of diluted sample or GSH standard was added per well and 120 µL of a 1:1 mixture of the DNTB and glutathione reductase stocks solutions was added to each assayed well. After 30 sec incubation, 60 µL of the NADPH was added and absorbance was immediately measured at 412 nm in 30 sec intervals for a total of 2 min. To determine the concentration of oxidized glutathione (GSSG), the samples were first diluted (1 in 4) in KPE and treated with 0.2 % 2-vinylpyridine for 1 h at room temperature. Excess vinyl-pyridine was quenched with 1 % triethanolamine and GSSG was measured using the same method as total glutathione except GSH standards were replaced with GSSG standards (0-26.24 nM/mL) that were treated with vinyl-pyridine and triethanolamine. The absolute values of total glutathione (GSH + GSSG) and oxidized glutathione (GSSG) per sample were calculated using the linear regression obtained from the change in absorbance/min plotted against the GSH or GSSG standard concentrations, respectively, and dividing by the total protein concentration. Absolute values for GSH were determined using the following equation: GSH= [GSH + GSSG] – 2[GSSG] [55].

Parkin-catalyzed redox state recycling

Parkin protein buffer exchange to T200 protein buffer (50 mM Tris, 200 mM NaCl, pH 7.5) was first performed using repeat centrifugations (8 times 4000 x g at 4°C for 10 min) in Amicon Ultra 10 kDa MWCO filters. Protein concentration was adjusted to 10 µM using T200. Both reduced (GSH) and oxidized (GSSG) glutathione stocks were prepared in phosphate buffered saline at concentrations of 1 mg/mL (3250 µM) and 2.01 mg/mL (6560 µM) respectively. Glutathione standards of 0, 2.5, 5, 10 µM and 100 µM of both GSH and GSSG were prepared and combined in the following ratios to a final volume of 90 µL at: 10 µM GSH: 0 µM GSSG, 9 µM GSH: 1 µM GSSG, 8 µM GSH: 2 µM GSSG, 6 µM GSH: 4 µM GSSG, 4 µM GSH: 6 µM GSSG, 2 µM GSH: 8 µM GSSG, 1 µM GSH: 9 µM GSSG, and 0 µM GSH: 10 µM GSSG. R-parkin (1 µL of a 10 µM solution) was added to the prepared mixtures and allowed to incubate at room temperature for 15 min. Samples were analyzed for GSH concentration using the monochlorobimane assay described above.

Glutathionylation assay

Glutathionylation of tagged and untagged parkin proteins was performed, as described previously [56]. MBP-tagged parkin proteins were eluted from columns with excess maltose. Concentrated eluates were supplemented with 0.1% DMSO (10 µl DMSO in 10 ml PBS), and excess DTT and maltose were removed by several cycles of centrifugation with 30 kDa cut-off filters. Proteins/peptides (14 µM) were incubated with 3 mM GSH for 1 h and then with 5 mM GSSG for 2 h at room temperature. Trypsin digestion was performed (Peptide: Trypsin = 20: 1) overnight at 4 °C. The Trypsin-digested fragments were run through MALDI analysis. To assay S-glutathionylation, the eosin-labeled GSSG (Di-E-GSSG) was used to glutathionylate proteins, as described previously [33]. Di-E-GSSG has quenched fluorescence in the disulphide form, which increases ~20-fold upon reduction of its disulphide bond and formation of E-GSH. Blackened 96-well-plates were used in a PerkinElmer Victor3 multilabel counter containing a final well volume of 200 µl in 0.1 M potassium phosphate buffer (pH 7.5), 1 mM EDTA. The reaction was started

by addition of 20 μM Di-E-GSSG to parkin proteins, followed by recording the fluorescence emission at 545 nm after excitation at 520 nm. Controls with no peptide added were used as fluorescent background. To confirm S-glutathionylation, reaction products were incubated with Di-E-GSSG. Aliquots of S-glutathionylated proteins were further treated with 10 mM DTT or with the complete GSH-Grx system. All samples were run on a non-reducing SDS-PAGE 4–12% acrylamide. The gel was exposed to UV transilluminator to visualize eosin-tagged glutathionylated protein. The same gels were later stained with Coomassie Blue staining. Di-Eosin-GSSG was purchased form IMCO, Sweden. Human Grx1, and Grx2 were prepared as described previously [33]. Rat recombinant TrxR was a kind gift from Prof. Elias Arner.

Protein carbonyl assay

Protein carbonyl colorimetric assay kit (Cayman chemical 10005020) was used to assay the carbonyl content in human and mouse brains or hearts. Pre-weighed tissues were rinsed in PBS and then homogenized in 1 mL cold PBS at pH 6.7 supplemented with 1 mM EDTA, using a Dounce homogenizer on ice. Homogenates were centrifuged at 10,000xg for 15 minutes at 4 °C. 200 μL of the supernatant was added to a tube with 800 μL DNPH (sample tube) and 200 μL of the supernatant was added to a tube with 800 μL 2.5 M HCL (control tube), both tubes were incubated in the dark for 1 hour with occasional vortex. 1 mL 20 % TCA followed by 1 mL 10% TCA solutions were added to centrifuged (10,000xg 10 minutes at 4 °C) pellet after discarding the supernatant. The resulting pellet was resuspended in1 mL of 1:1 ethanol:ethyl acetate mixture and centrifuged 3 times to extract protein pellets. The final pellets were suspended in 500 μL guanidine hydrochloride and centrifuged. A total of 220 μL per sample and control supernatants were added to two wells of a 96-well plate, and the absorbance was measure at 360 nm. The corrected absorbance (sample – control) was used in the following equation to obtain the protein carbonyl concentration: Protein Carbonyl (nmol/mL) = $[(CA)/(0.011\ \mu M^{-1})](500\ \mu L/200\ \mu L)$. Total protein concentration from the sample tissues were measured to obtain the carbonyl content: protein carbonyl/total protein concentration.

MnSOD activity assay

Superoxide dismutase assay kit (Cayman chemical 706002) was used to assay MnSOD activity in mouse brains. Pre-weighed perfused mouse brain pieces were homogenized in 5 mL cold 20 mM HEPES buffer, pH 7.2, supplemented with EGTA, mannitol and sucrose, with a Dounce homogenizer on ice. The homogenates were centrifuged at 1,500xg 5 minutes at 4 °C. The SOD standards were prepared by adding 200 µL of the radical detector and 10 µL of the provided standards, in duplicates in a 96-well plate. The same was repeated for the samples. The reaction was initiated by adding 20 µL of xanthine oxidase to all the wells. Background absorbance was assayed by adding 20 µL xanthine oxidase to sample buffer (optional). The plate was incubated on a shaker for 30 minutes at room temperature. The absorbance was measure at 450 nm. The linearized SOD standard curve was plotted and used to calculate the MnSOD activity (U/mL) from the averaged sample absorbances.

Total RNA isolation, cDNA synthesis and PCR amplification

Pre-weighed cortex pieces from mouse brains were homogenized in QIAzol (Qiagen 79306), at 1ml volume per 100mg of tissue, and incubated at room temperature for 5 minutes. 0.2mL of chloroform (per 1mL QIAzol) was added and the homogenates were shaken vigorously for 15 seconds, followed by a 2-3 minutes incubation at room temperature, the tubes were centrifuged at 12,000xg for 15 minutes at 4°C. The upper clear aqueous layer was transferred to a new tube and 1 volume of 70% ethanol was added, and mixed by vortexing. The solution was then added to an RNAeasy Mini spin column (Qiagen 74104) placed in a 2mL collection tube and centrifuged for 15 sec at 8000xg at room temperature. The flow-through was discarded and 700 µL Buffer RW1 was added to the spin column and spun for 15 sec at 8,000xg. The same step was repeated with 500 µL Buffer RPE, one spin for 15 sec and a second spin for 2 min. An optional spin in a new collection tube at full speed for 1 min to remove excess buffer was be added. The RNAeasy Mini spin column was placed in a new collection tube, 50 µL RNase-free water was added directly to the membrane and centrifuged for 1 minute at

8000xg. A NanoDrop machine was used to measure the amount of total RNA obtained from the cortices. Turbo DNA-free™ (Life Technologies 1412059) was used to remove trace to moderate amounts of contaminating DNA. SuperScrpit™ IV First-Strand Synthesis System (Invitrogen 18091050) was used for cDNA synthesis reaction. iTaq™ Universal SYBR® Green Supermix (BIO-RAD 172-5121) and select primer sets were used for PCR amplification of the newly synthesized cDNA templates, and controls, and analyzed by agarose gel electrophoresis and ethidium bromide staining. The following primers were used [57-59]:

DJ-1, F: ATCTGAGTCGCCTATGGTGAAG; R: ACCTACTTCGTGAGCCAACAG

GCLC, F: ATGTGGACACCCGATGCAGTATT; R: TGTCTTGCTTGTAGTCAGGATGGTTT

GCLM, F: GCCACCAGATTTGACTGCCTTT; R: CAGGGATGCTTTCTTGAAGAGCTT

Actin, F: CTTCCTCCCTGGAGAAGAGC; R: AAGGAAGGCTGGAAAAGAGC

Statistical analyses

All statistical analyses were performed using GraphPad Prism version 8 (GraphPad Software, San Diego, CA, USA, www.graphpad.com). Differences between two groups were assessed using an unpaired t-test. Differences among 3 or more groups were assessed using a one-way or two-way ANOVA followed by Tukey's post hoc corrections to identify statistical significance. Subsequent post hoc tests are depicted graphically and show significance between treatments. For all statistical analysis a cut-off for significance was set at 0.05. Data is displayed with p values represented as *$p < 0.05$, **$p < 0.01$, ***$p < 0.001$, and ****$p < 0.0001$.

MATERIALS AND METHODS REFERENCES

52 Hu, J. & Li, S. Electroporation formulation for cell therapy. *Methods Mol Biol* **1121**, 55-60, doi:10.1007/978-1-4614-9632-8_4 (2014).

53 Kumar, A. *et al.* Disruption of the autoinhibited state primes the E3 ligase parkin for activation and catalysis. *EMBO J* **34**, 2506-2521, doi:10.15252/embj.201592337 (2015).

54 Matsuda, N. *et al.* Diverse effects of pathogenic mutations of Parkin that catalyze multiple monoubiquitylation in vitro. *J Biol Chem* **281**, 3204-3209, doi:10.1074/jbc.M510393200 (2006).

55 Rahman, I., Kode, A. & Biswas, S. K. Assay for quantitative determination of glutathione and glutathione disulfide levels using enzymatic recycling method. *Nat Protoc* **1**, 3159-3165, doi:10.1038/nprot.2006.378 (2006).

56 Casagrande, S. *et al.* Glutathionylation of human thioredoxin: a possible crosstalk between the glutathione and thioredoxin systems. *Proc Natl Acad Sci U S A* **99**, 9745-9749, doi:10.1073/pnas.152168599 (2002).

57 Diaz, D. *et al.* Tissue specific changes in the expression of glutamate-cysteine ligase mRNAs in mice exposed to methylmercury. *Toxicol Lett* **122**, 119-129, doi:10.1016/s0378-4274(01)00341-1 (2001).

58 Shi, S. Y. *et al.* DJ-1 links muscle ROS production with metabolic reprogramming and systemic energy homeostasis in mice. *Nat Commun* **6**, 7415, doi:10.1038/ncomms8415 (2015).

59 Abelev, B. I. *et al.* Longitudinal double-spin asymmetry and cross section for inclusive jet production in polarized proton collisions at square root of s = 200 GeV. *Phys Rev Lett* **97**, 252001 (2006).

ACKNOWLEDGMENTS

We are grateful for the commitment of patients and their family members to participate in autopsy studies. We thank Drs. A. Brice and E. Fon for sharing *prkn*-null mice, Drs. N. Matsuda and K. Tanaka for MBP-parkin cDNA-encoding plasmids; Drs. R. Tam, S. Bennett and D. Pratt for helpful discussions, members of the Schlossmacher lab for their critical comments including Dr. T. Kitada for the suggestion to study *Sod2*$^{+/-}$ animals. **Funding:** This work was supported by the: Parkinson Research Consortium of Ottawa (D.N.E.K., J.M.T., J.J.T.); Queen Elizabeth II Graduate Scholarship Fund (J.M.T.); Government of Canada [NSERC (J.K.); CIHR MD/PhD Program (J.M.T., A.C.N.); NINDS/NIH (to M.J.L.); CIHR Research Grants (G.S.S., M.E.H.); CIHR Canada Research Chair Program (M.G.S.; G.S.S.)]; Michael J. Fox Foundation for Parkinson's Research (J.J.T., L.Z., M.G.S.); Uttra and Sam Bhargava Family (M.G.S.); and The Ottawa Hospital (M.G.S.). **Author contributions:** *Study design:* D.N.E.K., J.M.T., J.J.T., M.G.S.; *Writing and figure preparation:* D.N.E.K., J.M.T., N.A.L. and M.G.S. prepared the initial draft of the manuscript and figures. All authors reviewed and / or edited the manuscript and approved of the submitted version. *Experiments*: D.N.E.K., J.M.T., N.A.L., R.S., A.C.N., H.B., C.P., B.S., D.S.I., L.Z., and L.P. performed experiments; R.S., C.P, J.A.C, M.T, N.H., R.R.R. and L.P provided data, tissue specimens and critical comments. *Analysis:* D.N.E.K. J.M.T, J.L., J.J.T., and M.G.S. performed data analyses. *Study supervision*: J.J.T. and M.G.S. *Overall responsibility:* M.G.S. This work is dedicated to the memories of Mr. Bruce Hayter (1962-2019), a tireless advocate for persons with young-onset parkinsonism, and our colleague, Dr. Arne Holmgren (1940-2020), a pioneer in redox biology.

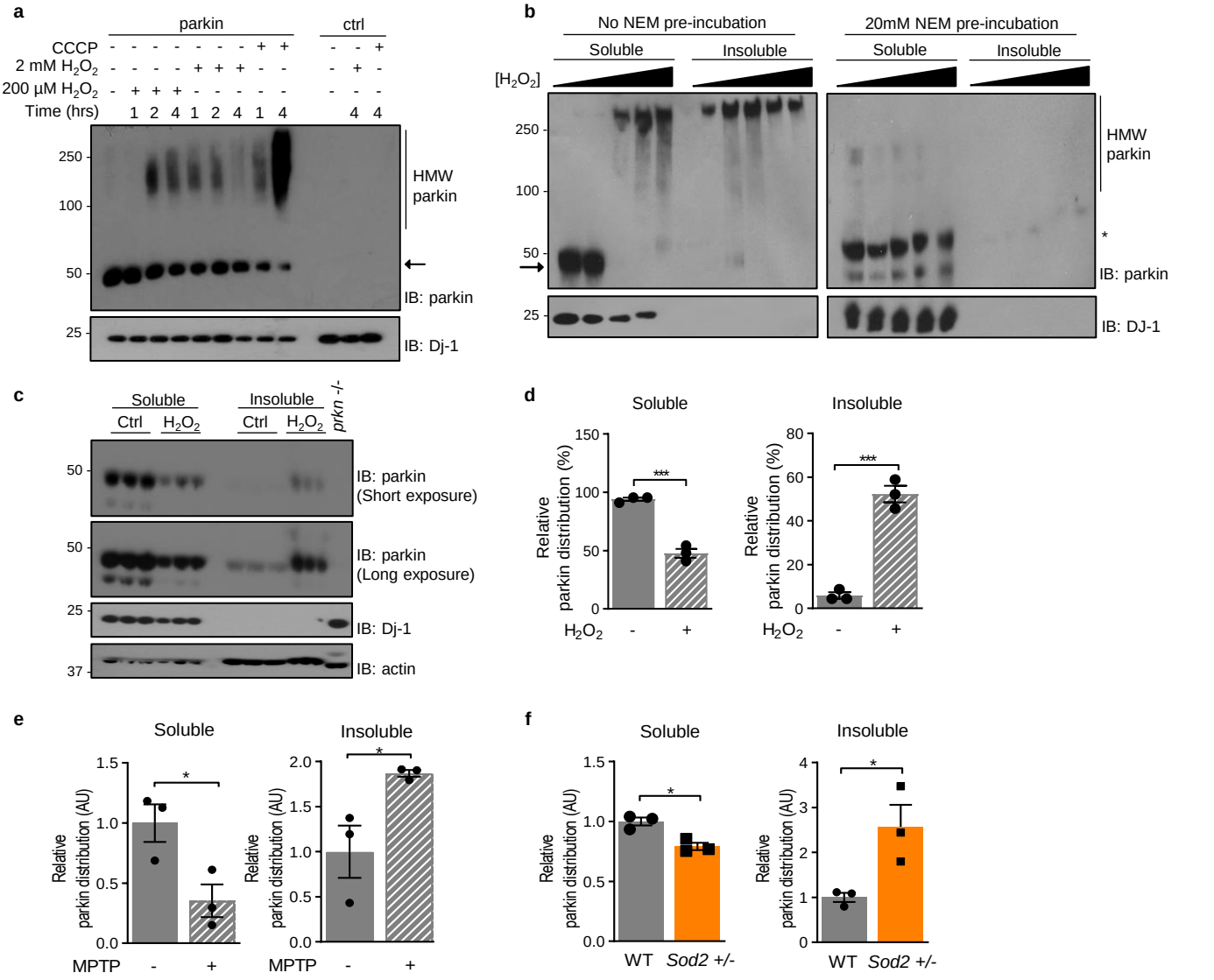

Figure 1:Mitochondrial and cytosolic stressors lead to oxidation of cellular parkin promoting its insolubility. **a**, Chinese hamster ovary cells (CHO) wild-type or stably expressing myc-parkin were cultured under increasing concentrations of stressors (200µM and 2mM H_2O_2; and 10µM CCCP) for 1, 2 or 4 hours. Cell lysates were run on SDS gels and immunoblotted for parkin and DJ-1 as control. (←) Monomeric parkin. **b**, Human embryonic kidney cells (HEK293) ectopically expressing flag-parkin incubated with increasing concentrations of H_2O_2 (2µM to 2M) for 30 minutes with or without a 15 minutes 20mM N-ethylmaleimide (NEM) pre-incubation (to block all available cysteine residues) were lysed and separated into a soluble (salt-extracted) and insoluble (2-10%SDS-extracted) fractions. (*) Alkylated-parkin. **c,** 2-4 months old wild-type C57Bl/6 mouse brains were incubated with saline or 1% H_2O_2. Brain homogenates were separated into soluble and insoluble fractions and **d,** parkin's signal distribution was quantified using image-J densitometry. **e,** 2-4 months old wild-type C57Bl/6 mice were administered either a 40mg/Kg single intraperitoneal injection of the dopaminergic cell-specific neurotoxin 1-methyl-4-phenyl-1,2,3,6-tetrahydropyridine (MPTP) or saline, and sacrificed an hour later (Ali et al., 1994). Parkin's signal distribution was quantified using image-J and controlled for loading, in the soluble fraction and the insoluble one. **f**, Brain homogenates from C57Bl/6 wild-type and *Sod2*$^{+/-}$ mice were fractioned and parkin's signal was quantified in the soluble fraction and the insoluble one. A student t-test was used for statistical analysis (* = < 0.05, *** = <0.001).

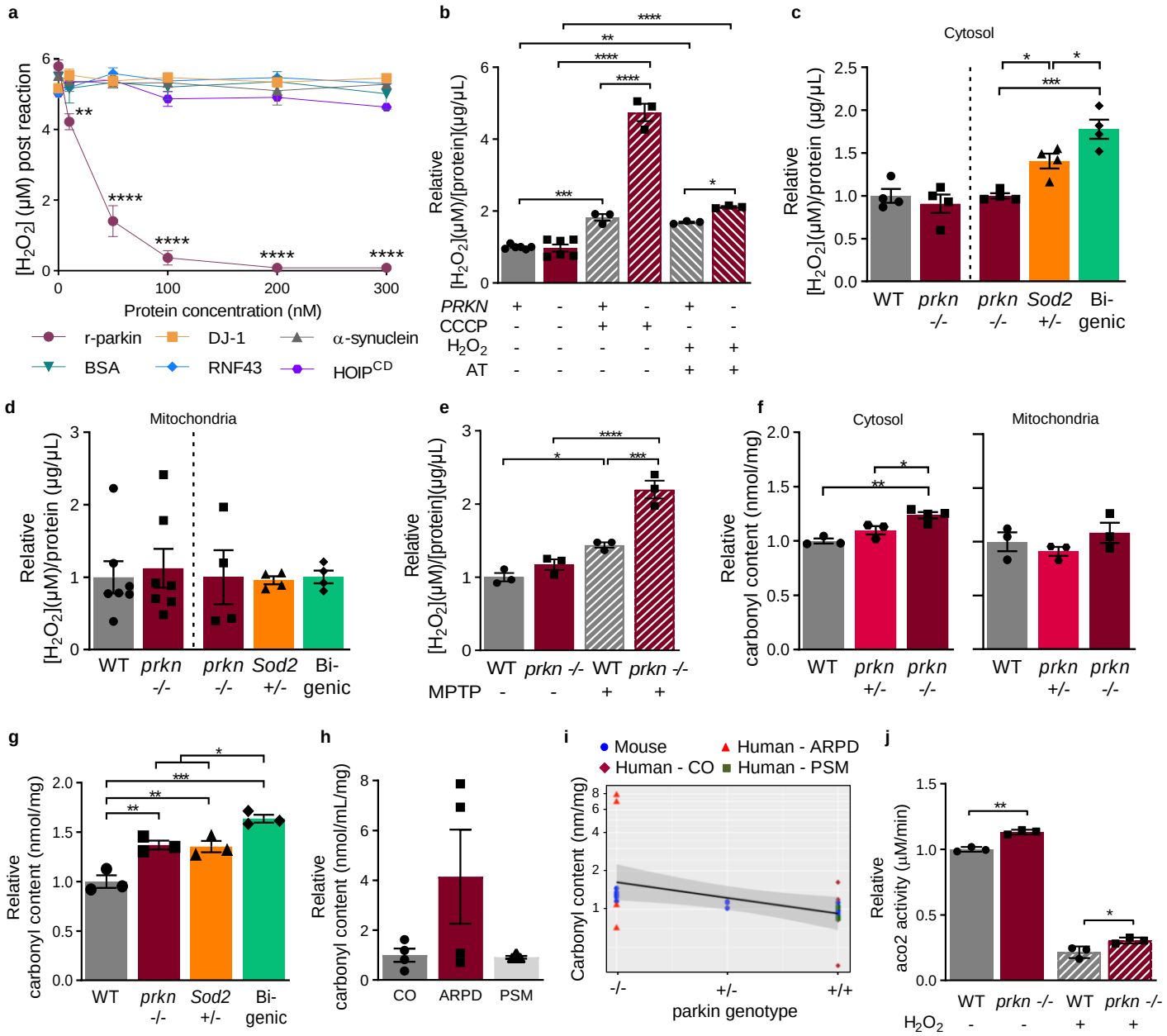

Figure 2:Parkin's cysteine-dependent redox capacity lowers hydrogen peroxide to reduce oxidative stress. **a,** Parkin's reducing capacity was assessed compared to two PD-linked proteins (DJ-1 and α-synuclein), BSA and two RING-carrying ubiquitin ligases (RNF43 and HOIP^{cd}). **b,** Cellular redox state was assessed by measuring endogenous levels of hydrogen peroxide in HEK293 cells overexpressing flag-parkin or flag-vector under control conditions, with 10μM carbonyl cyanide m-chlorophenyl hydrazine (CCCP) incubation for 1 hour, or with the addition of 0.5M aminotriazole (AT, to block catalase) and 2mM H_2O_2 incubation for 30mins**.** Endogenous levels of hydrogen peroxide were measured in **c,** cytosolic-dominant and **d,** mitochondrial-dominant brains homogenates of 6-8 months old wild-type and *prkn*$^{-/-}$ and, 2-4 months *prkn*$^{-/-}$, *Sod2*$^{+/-}$ and bigenic (*prkn*$^{-/-}$//*Sod2*$^{+/-}$) C57Bl/6 mice. **(E)** H_2O_2 levels were assayed in WT or *prkn*$^{-/-}$ mouse brains treated *in vivo* with either saline or MPTP. Protein carbonyl content, an H_2O_2-dependent irreversible marker of oxidative stress, was measured in **f,** cytosolic-dominant and mitochondrial-dominant fractions of 8 months old WT, *prkn*$^{+/-}$, and *prkn*$^{-/-}$ mouse brains, **g,** hemibrain homogenates of 6 months old WT, *prkn*$^{-/-}$, *Sod2*$^{+/-}$ and bigenic mice, and **h,** aged-matched control, *PRKN*-deficient and parkinsonian human cortices. **i,** Logistic regression analysis of carbonyl content as a function of parkin's presence for mammalian brains (human and mouse; each brain is represented by an individual dot); the logistic regression line (in black) and 95% confidence intervals (grey) are shown. **j,** Aconitase-2 enzymatic activity was assayed in mitochondria isolated from WT and *prkn*$^{-/-}$ mouse brains. 1way or 2way ANOVA was used for statistical analysis (* = < 0.05; ** = < 0.01; *** = < 0.001; and ****= <0.0001).

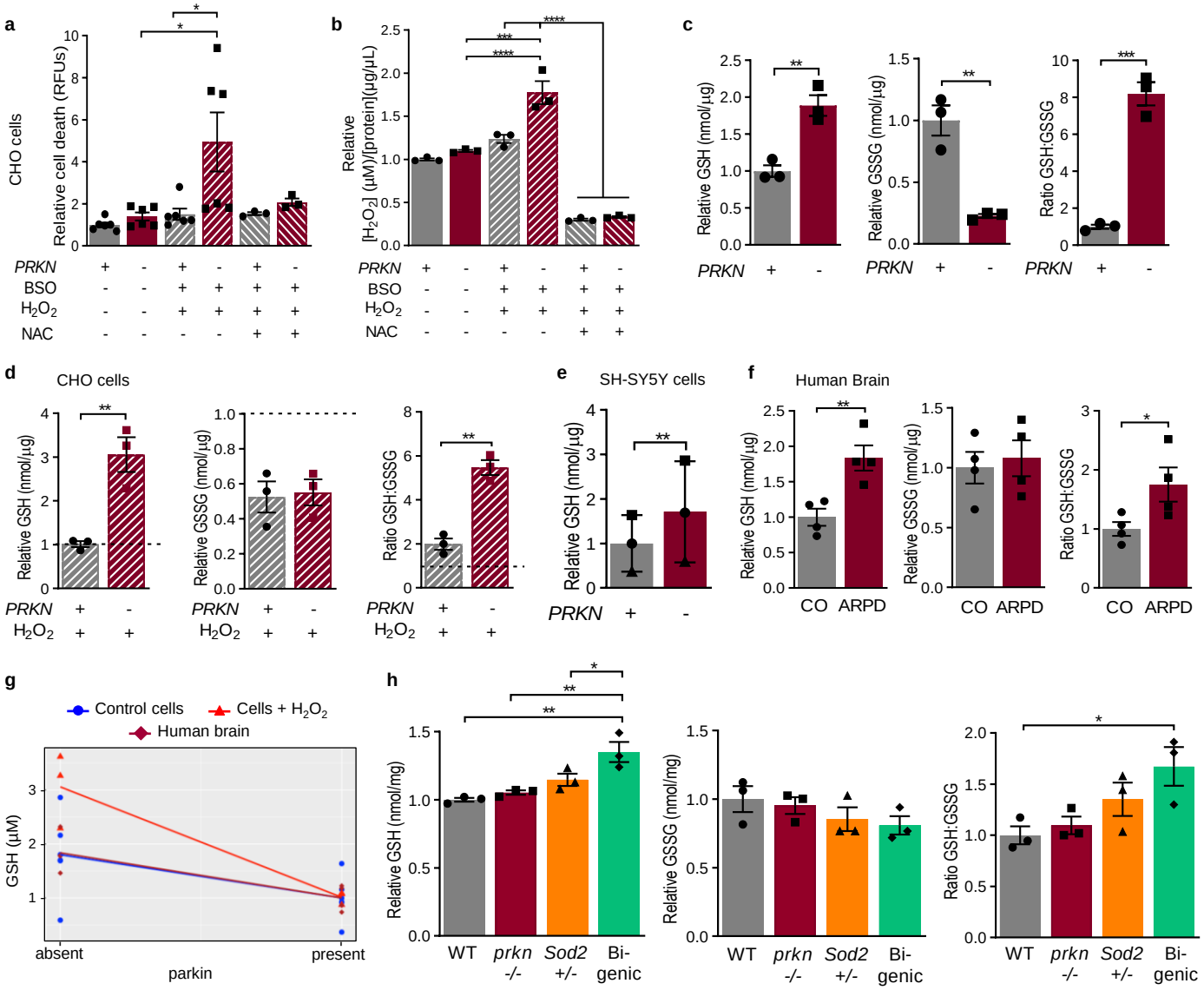

Figure 3:| *PRKN* expression alters glutathione metabolism in cells and human brain.
Cellular toxicity **a,** and endogenous H_2O_2 levels **b,** were assayed in in WT CHO or CHO-parkin cells under control conditions or with dual exposure to 2 mM H_2O_2 and 2mM BSO, with or without supplementation by 20mM NAC. Free, reduced levels of glutathione (GSH), oxidized glutathione (GSSG), and the GSH:GSSG ratio were assayed by HPLC in CHO and CHO-parkin cells under **c,** control conditions, and **d,** post H_2O_2 stress. **e,** Reduced GSH levels were assayed in SHSY5Y cells under control conditions, using the MCB method. The same readouts were measured using HPLC in **f,** control and *PRKN* deficient human brain cortices, and **h,** brains of 6 months old WT, *prkn* -/-, *sod2* +/- and bigenic mice. **g**, Logistic regression analysis of reduced GSH levels as a function of parkin's presence for human brains and CHO cells under basal and oxidizing conditions; the logistic regression lines are shown. A student t-test and 1way ANOVA were used for statistical analysis (* = < 0.05; ** = < 0.01; and *** = < 0.001).

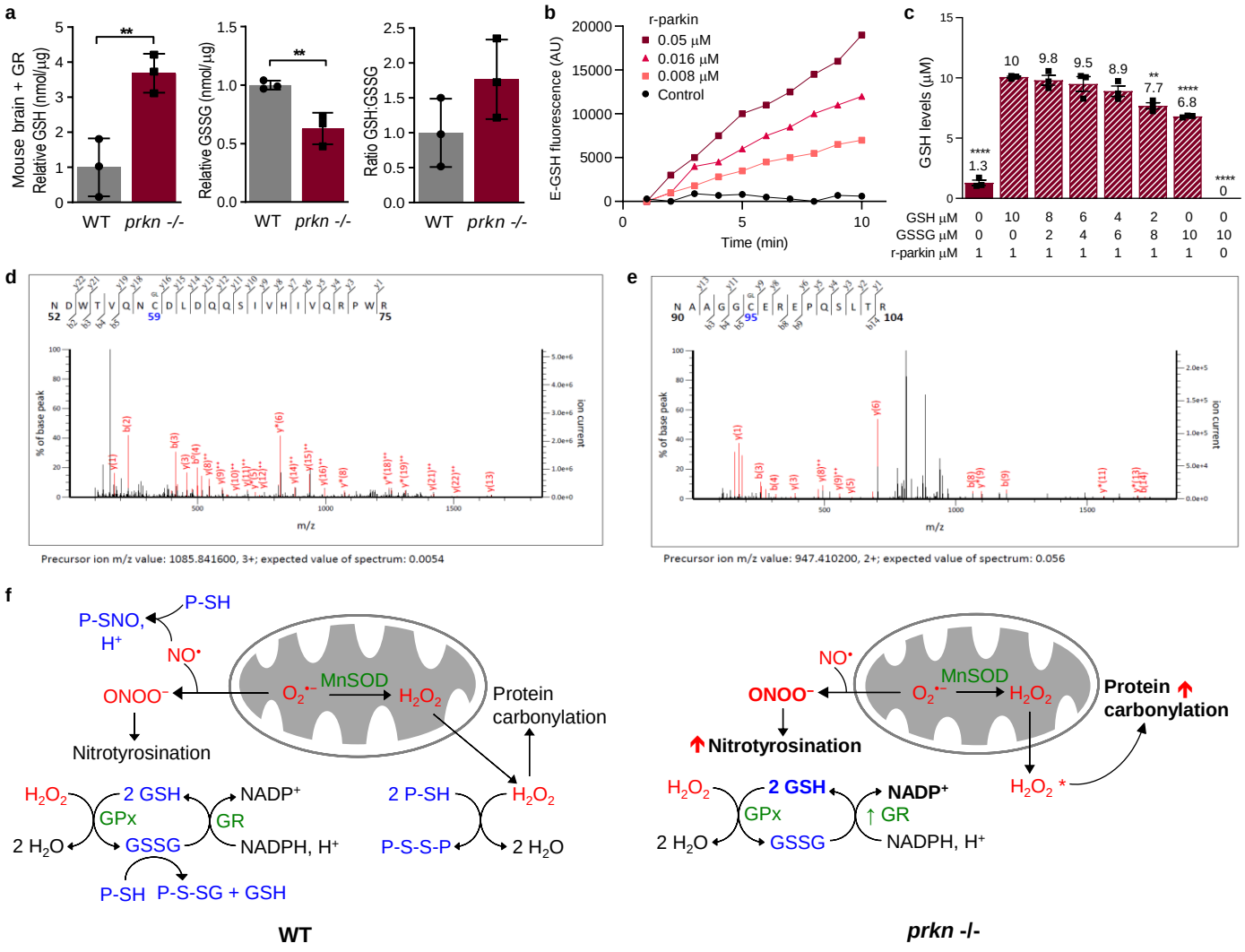

Figure 4:Parkin contributes to glutathione recycling independent of *de novo* synthesis.
a, Using the GR-dependent Tietze method, reduced GSH, oxidized GSSG, and GSH:GSSG ratio were assayed in 8-12 months old WT and *prkn*$^{-/-}$ mouse brains. **b,** Recombinant, full-length, MBP-parkin was treated with 20 µM Di-E-GSSG and the release of E-GSH measured at 545 nm after excitation at 520 nm. The fluorescence increase of Di-E-GSSG (black circle) was used as background. **c**, Indicated levels of untagged glutathione preparations (µM) at various GSH:GSSG ratios were incubated with 1 µM of tag-less, full-length r-parkin. Levels of free GSH were measured using monochlorobimane (mcB) assay. A one-way Anova with Dunnett's post hoc test was used to compare all values to r-parkin incubated with 10 µM GSH (**** p<0.0001, n=3). A student t-test or 1way ANOVA was used for statistical analysis (* = < 0.05; ** = < 0.01; and *** = < 0.001). **d-e**, Examples of LC-MS/MS-generated spectra following trypsin digestion of MBP-parkin incubated with Di-E-GSSG. **d**, Human parkin peptide aa52-75 is shown, with cysteine 59 S-glutathionylated. **e,** Human parkin peptide aa90-104 is shown, with cysteine 95 S-glutathionylated. **f,** Graphical depiction of redox changes including: GSH recycling; generation of ROS levels (*i.e.*, H_2O_2; superoxide) leading to carbonylation; metabolism of nitric oxide (NO) leading to nitrotyrosination; and function of select enzymes in *WT vs.* parkin-deficient (*prkn*$^{-/-}$) mammalian brain. P, parkin; MnSOD, Mn^{2+}-dependent superoxide dismutase; GPx, glutathione peroxidase; GR, glutathione reductase. * indicates evidence from human brain[11].

Run	1		2		Mean	
Treatment	Saline (n=1)	MPTP (n=1)	Saline (n=2)	MPTP (n=2)	Saline	MPTP
Number of unique parkin peptides identified	11	18	11	27	11.0	22.5
Number of amino acids identified	106	154	123	323	114.5	238.5
% coverage	23	33	27	70	25.0	51.5
Number of cysteines identified	6	10	7	26	6.5	18.0
% of total cysteines	17.6	29.4	20.6	76.5	19.1	52.9
Number of IAA-modified cysteines identified	6	8	7	22	6.5	15.0
Ratio IAA-cysteines/total cysteines identified	100.0	80.0	100.0	84.6	100.0	82.3
Cysteine -> Dehydroalanine	C195	C195	C195, C240, C252	C195, C237, C240, C252, C376		
Sulfonic acid (Cys trioxidation)	C252	C252	C252, C417, C420	C211, C252		
Sulfinic acid (Cys dioxidation)	n/d	n/d	n/d	C252		
Phosphorylation	n/d	n/d	n/d	S77		
Methionine oxidation	M191, M457	M191, M457	M191, M457	M191, M326, M457		

Extended Data Table 1: Parkin cysteines are oxidized in adult mouse brain

Table summarizing mass spectrometry results highlighting the ratios of the number of IAA-tagged and free cysteines divided by the total number of identified cysteines in wild-type parkin enriched from the brains of mice treated with MPTP (2 independent runs, n=3 brains each) compared to saline controls (2 independent runs, n=3 brains each) under reducing and alkylating conditins (see text for details). The means of both runs in each treatment are shown with the ratio (in percent) of IAA-tagged cysteines to total identified cysteines highlighted. Select, oxidative stress-induced, posttranslational modifications of mouse parkin's cysteines are included at the bottom, *e.g.*: cysteine to dehydroalanine, cysteine dioxidation (=sulfinic acid) and cysteine trioxidation (=sulfonic acid). Phosphorylation as well as methionine oxidation events are also indicated.

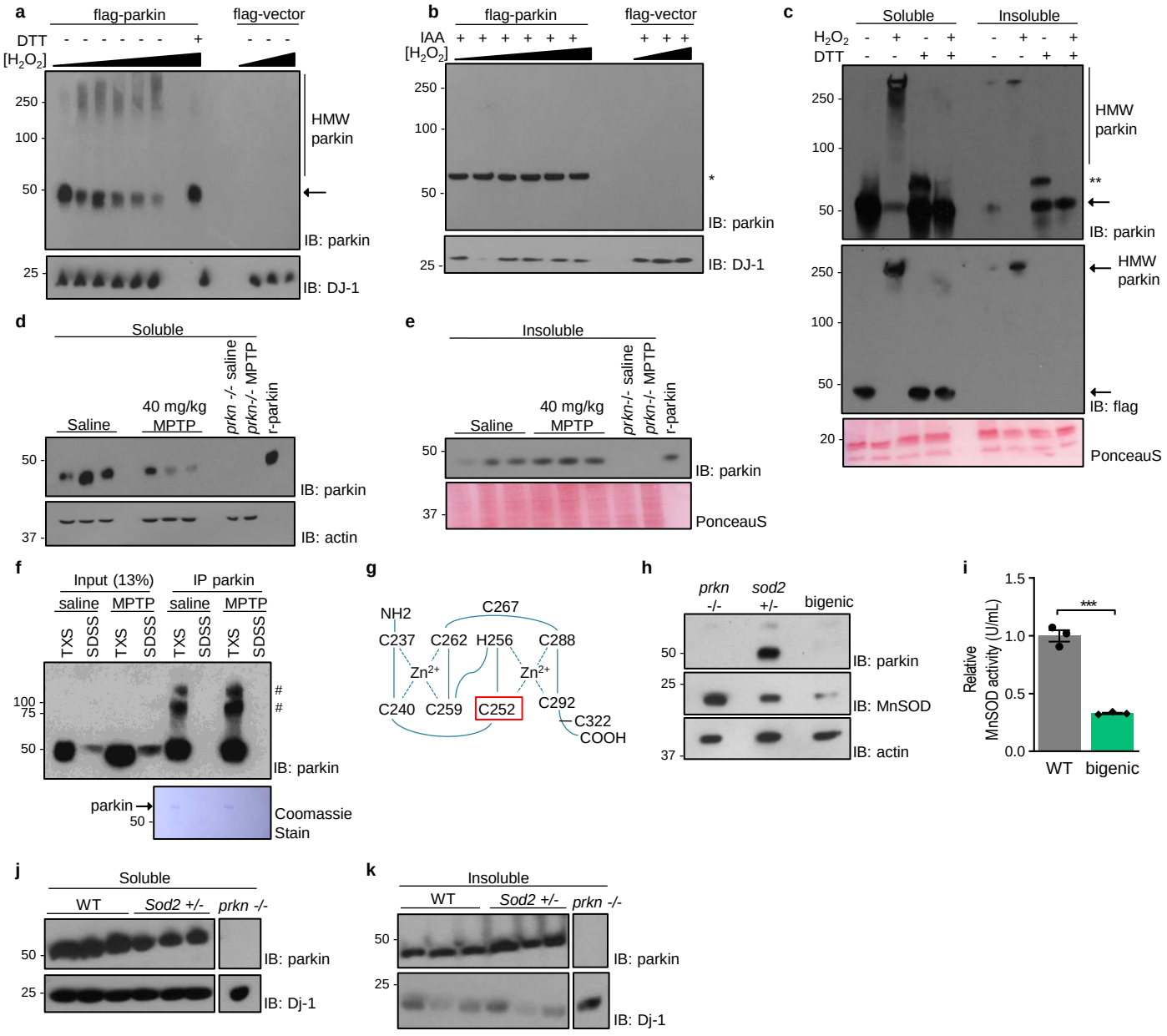

Extended Data Figure 1:Mitochondrial and cytosolic stressors lead to oxidation of cellular parkin promoting its insolubility.

HEK293 wild-type and ectopically expressing flag-parkin or flag-vector were incubated with increasing concentrations of H_2O_2 (2μM to 20mM) **a,** in the presence of a reducing agent DTT for 30 minutes or **b,** pre-incubating with 100mM iodoacetamide (IAA) for 15 minutes to block free available cysteines. **c,** Parkin's HMW formation and shift in solubility was visualized by immunoblotting for parkin and flag lysates from HEK293 cells ectopically overexpressing flag-parkin under oxidizing and/or reducing conditions**.** Recombinant human parkin (r-parkin) myc-tagged. (←) Monomeric parkin, (*) Alkylated-parkin and (**) DTT-modified-parkin. Whole or hemi brain homogenates from mice treated with either saline or MPTP were separated into soluble **d,** and insoluble **e,** fractions ran on SDS gel and immunoblotted for parkin and DJ-1 or Ponceau S for control. **f,** Using parkin antibody conjugated beads we pulled down parkin from mouse brains after treatment with saline or MPTP. Immunoprecipitation products were separated by reducing SDS/PAGE and visualized by Coomassie blue stain, bands were excised and submitted to mass spectrometry analysis. (#) IgG related bands. **g,** Schematic representation of parkin's RING1 domain with the position of an oxidized cysteine residue highlighted (C252). **h,** Brain homogenates from 2-4 months old *prkn*$^{-/-}$, *Sod2*$^{+/-}$ and bigenic mice were run on reducing SDS/PAGE gels and immunoblotted for parkin, MnSOD and actin. **i,** MnSOD activity in brain homogenates from 2-4 months old WT and bigenic mice were assayed utilizing tetrazolium salt for detection of superoxide radicals generated by xanthine oxidase and hypoxanthine. Soluble **j,** and insoluble **k,** fractions of brain homogenates from WT and *Sod2*$^{+/-}$ mice were run on SDS gels and immunoblotted for parkin and DJ-1. A student t-test or 1way ANOVA was used for statistical analysis (*** = < 0.001).

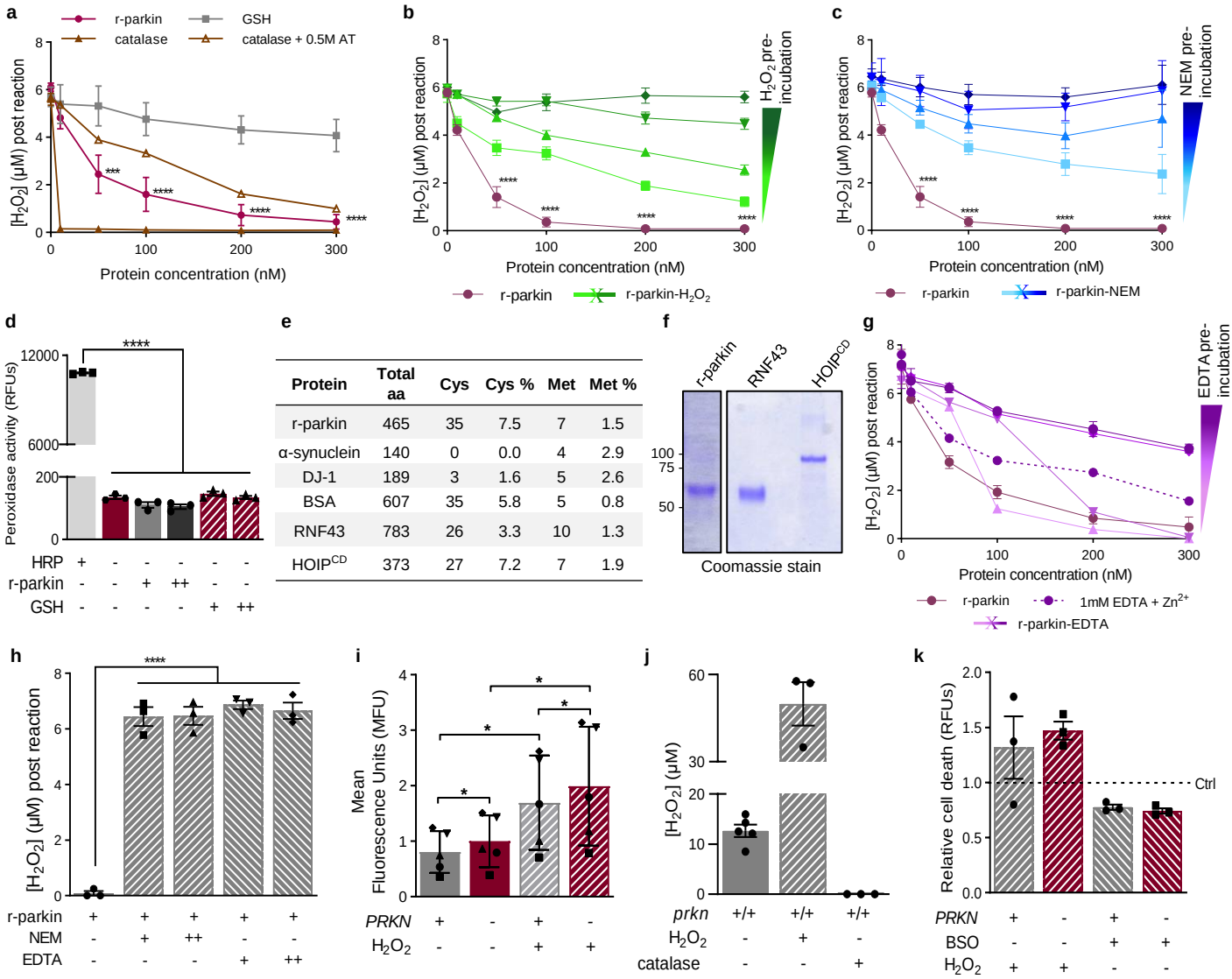

Protein	Total aa	Cys	Cys %	Met	Met %
r-parkin	465	35	7.5	7	1.5
α-synuclein	140	0	0.0	4	2.9
DJ-1	189	3	1.6	5	2.6
BSA	607	35	5.8	5	0.8
RNF43	783	26	3.3	10	1.3
HOIP^{CD}	373	27	7.2	7	1.9

Extended Data Figure 2:Parkin's cysteine-dependent redox capacity lowers hydrogen peroxide to reduce oxidative stress.

a, Parkin's reducing capacity was assessed compared to well-established cellular anti-oxidants, *i.e.*, glutathione and catalase, at equal molar concentrations. Aminotriazole was used to block catalase activity. Full-length, human, recombinant (r-) parkin's ability to interact with H_2O_2 was assessed **b,** post oxidization with increasing concentrations of H_2O_2 (range, 2μM to 2mM), and **c,** after incubating the protein with increasing concentrations of cysteine-specific blocker NEM (100μM to 1mM). **d,** Parkin and glutathione were tested regarding any peroxidase activity in comparison to horseradish peroxidase. **e,** Table summarizing the cysteine and methionine content of parkin, two PD-linked proteins (DJ-1; α-synuclein), bovine serum albumin (BSA) and two RING-positive E3 ubiquitin ligases (RNF43 and HOIP^{cd} (cd, catalytic domain)). **f,** Preparations of nascent r-parkin, RNF43 and HOIP^{cd} proteins were visualized by Coomassie stain after SDS/PAGE. **g,** Parkin's reducing capacity was assessed post incubation with increasing concentrations of ethylenediaminetetraacetic acid (EDTA; range, 100μM to 1mM) to chelate its structural zinc ions. **h,** H_2O_2 reducing capacity was assessed for NEM and EDTA, to confirm non-reactivity with the AmplexRed assay. **i,** Level of ROS measured by flow cytometry in living HEK293 cells treated with 0 or 2 mM H_2O_2 and exposed to dichlorofluorescin diacetate, DCFH-DA. Paired data are represented by a distinct symbol. Paired two-way ANOVA with Bonferroni post hoc test was used (* p=0.0295 showing differences between *PRKN* expression *vs.* control, p=0.0226 for the difference between H_2O_2 treated *vs.* non-treated samples, n=5). **j,** Assay sensitivity of measuring hydrogen peroxide using AmplexRed, as demonstrated by the addition of H_2O_2 or catalase to mouse brain homogenates. **k,** Cell cytotoxicity was assayed in WT CHO and CHO-parkin cells under normal conditions or with the addition 2mM H_2O_2 or 20mM BSO alone. A 1 or 2 way ANOVA analysis was used (*= <0.05; ** = < 0.01; ***= <0.001; and **** = <0.0001).

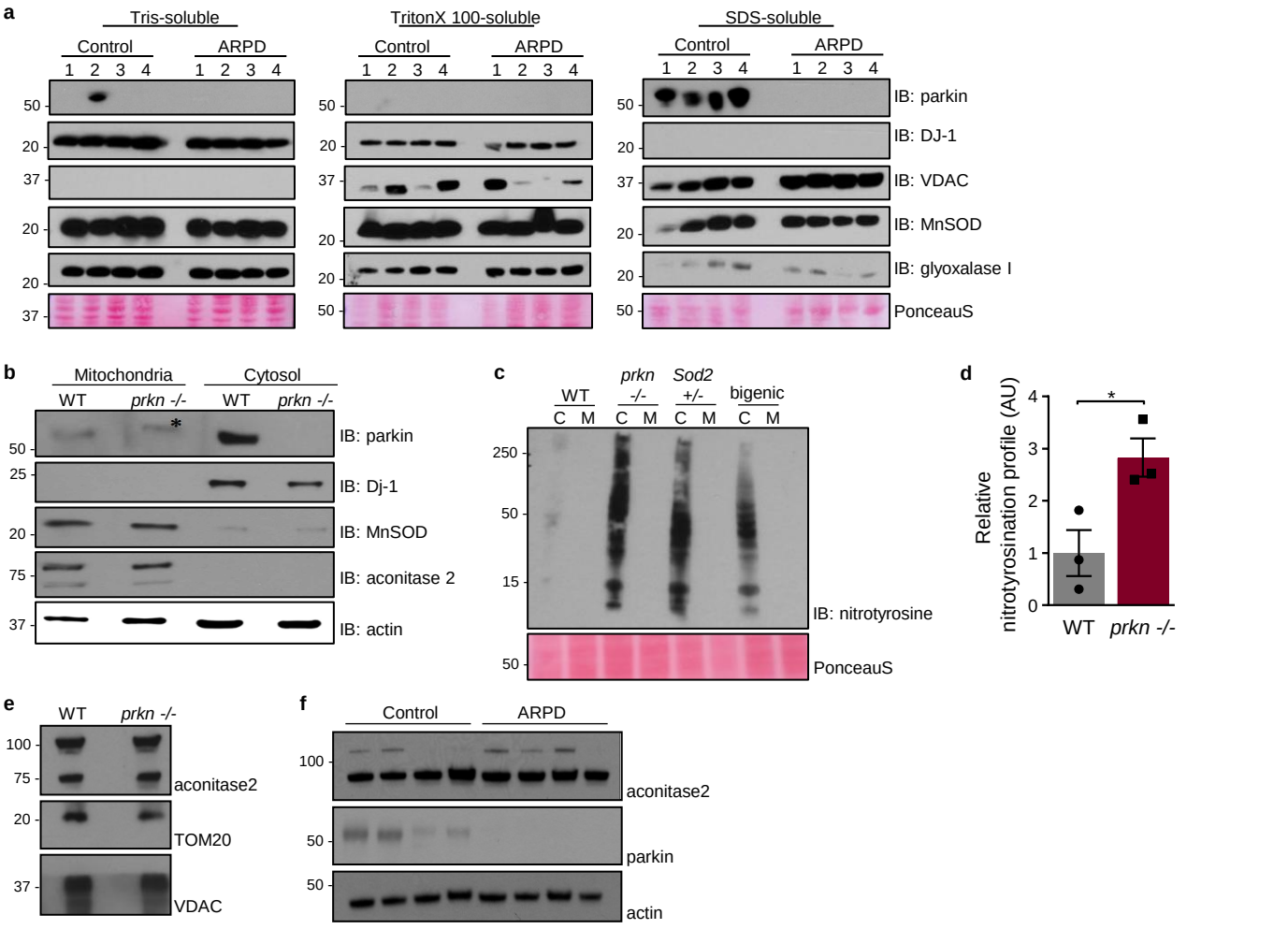

Extended Data Figure 3: *PRKN* expression alters glutathione metabolism in cells and human brain.
a, Aged-matched control and human ARPD (*PRKN* mutant) cortices, described in Shimura et al.[25], were serially fractioned using increasing concentrations of detergent to extract soluble (TS), lipid-bound (TX) and insoluble (SDS) fractions, as described[11]. Fractions were immunoblotted for parkin, DJ-1 and three mitochondria proteins, voltage-dependent anion channel (VDAC), manganese superoxide dismutase (MnSOD) and glyoxalase-1. **b,** Western blot analysis of mitochondria-enriched and cytosol fractions from WT and *prkn*$^{-/-}$ mouse brains, using parkin, Dj-1, MnSOD, aconitase-2 and actin as markers (* indicates non-specific band). **c,** Nitrotyrosination signals, which result from the peroxynitrite-dependent irreversible nitration of tyrosine groups of a protein (due to high levels of superoxide and its reaction with nitric oxide), from 6 months old WT, *prkn*$^{-/-}$, *Sod2*$^{+/-}$ and bigenic mice were analysed by immunoblotting heart muscle homogenates for nitrotyrosine. **d,** Quantification of nitrotyrosination signals in WT and *prkn*$^{-/-}$ mouse hearts. Aconitasse-2 protein levels were visualized in mitochondrial extracts from **e,** mouse brains, and **f,** human brains. A student t-test was used for statistical analysis (* = < 0.05).

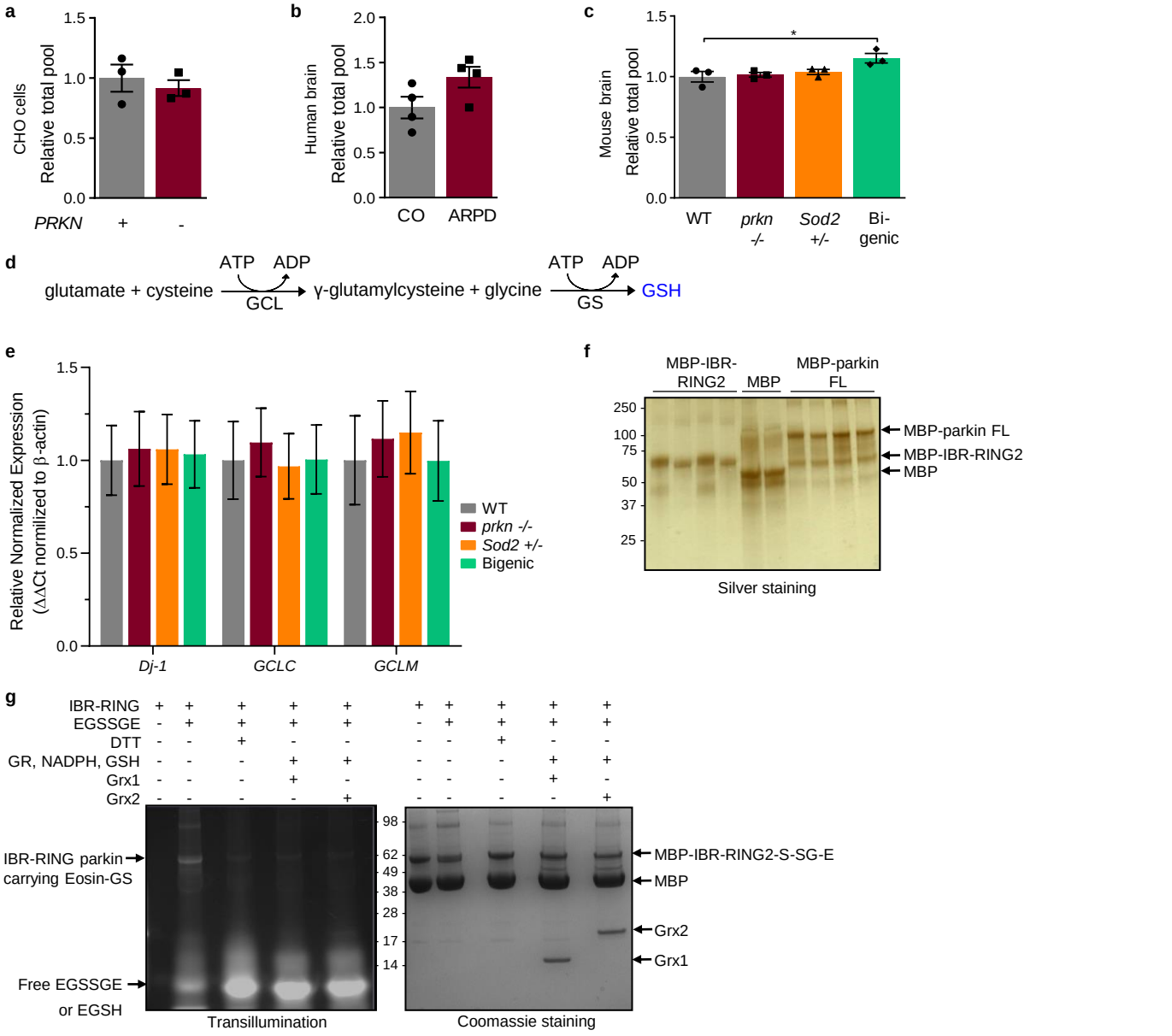

Extended Data Figure 4: Parkin contributes to glutathione recycling independent of *de novo* synthesis.
The total GSH + GSSG pool as measured by HPLC in **a,** CHO cells, **b,** human cortices, and **c,** brain homogenates of 6 mths-old WT, *prkn*$^{-/-}$, S*od2*$^{+/-}$, and bigenic mice. **d,** Graphic depiction of GSH synthesis from glutamate and cysteine, with GCL as the rate-limiting enzyme. **e,** *Dj-1*, *GCLC* and *GCLM* gene expression in brains of 6 mths old WT, *prkn*$^{-/-}$, *Sod2*$^{+/-}$ and bigenic mice. **f,** Silver stain after reducing SDS/PAGE of recombinantly expressed maltose binding protein (MBP)-tag and MBP-tagged parkin proteins, as indicated and used in glutathionylation studies. Lanes 1-4 contain MBP-IBR-RING2 (parkin, aa 327-465, ~60-65 kDa), lanes 5-6 contain MBP alone (~45-50 kDa) and lanes 7-10 contain MBP-FL-parkin (~90 kDa; aa1-465, 95 kDa). **g,** Glutathionylation studies using IBR-RING2. Previously redox reduced preparations of 10 μM MBP-IBR-RING2 parkin were treated with 20 μM Di-E-GSSG and release of E-GSH was monitored. After incubation, samples were run on non-reducing SDS/PAGE. After gel electrophoresis, MBP-IBR-RING2-S-SG-E was visualized via an UV transilluminator (left). The gel was subsequently stained with Coomassie Blue (right). Lane 1 (from left), untreated MBP-IBR-RING2; lane 2, MBP-IBR-RING2-S-SG-E; lane 3, DTT (5 mM)-treated aliquot of MBP-IBR-RING2-S-SG-E; lane 4, Grx1 system-treated aliquot of MBP-IBR-RING2-S-SG-E; lane 4, Grx2 system-treated aliquot of MBP-IBR-RING2-S-SG-E. The Grx1 system contained 1 μM Grx1 or Grx2, 1 mM NADPH, 5 mM GSH, and 0.1 μM GR enzyme. Results are representative of three independent experiments.